Human cortical–hippocampal dialogue in wake and slow-wave sleep

Anish Mitra[a,1], Abraham Z. Snyder[a,b], Carl D. Hacker[c], Mrinal Pahwa[c], Enzo Tagliazucchi[d,e], Helmut Laufs[e,f], Eric C. Leuthardt[g], and Marcus E. Raichle[a,b,1]

[a]Department of Radiology, Washington University in St. Louis, St. Louis, MO 63110; [b]Department of Neurology, Washington University in St. Louis, St. Louis, MO 63110; [c]Department of Biomedical Engineering, Washington University in St. Louis, St. Louis, MO 63110; [d]Institute for Medical Psychology, Christian Albrechts University Kiel, Kiel, Germany; [e]Department of Neurology and Brain Imaging Center, Goethe University Frankfurt, Frankfurt, Germany; [f]Department of Neurology, Christian Albrechts University Kiel, Kiel, Germany; and [g]Department of Neurosurgery, Washington University in St. Louis, St. Louis, MO 63110

Contributed by Marcus E. Raichle, August 22, 2016 (sent for review May 9, 2016; reviewed by Elizabeth A. Buffalo, Gyorgy Buzsáki, Yuval Nir, and Olaf Sporns)

Declarative memory consolidation is hypothesized to require a two-stage, reciprocal cortical–hippocampal dialogue. According to this model, higher frequency signals convey information from the cortex to hippocampus during wakefulness, but in the reverse direction during slow-wave sleep (SWS). Conversely, lower-frequency activity propagates from the information "receiver" to the "sender" to coordinate the timing of information transfer. Reversal of sender/receiver roles across wake and SWS implies that higher- and lower-frequency signaling should reverse direction between the cortex and hippocampus. However, direct evidence of such a reversal has been lacking in humans. Here, we use human resting-state fMRI and electrocorticography to demonstrate that δ-band activity and infraslow activity propagate in opposite directions between the hippocampus and cerebral cortex. Moreover, both δ activity and infraslow activity reverse propagation directions between the hippocampus and cerebral cortex across wake and SWS. These findings provide direct evidence for state-dependent reversals in human cortical–hippocampal communication.

hippocampus | cortex | sleep | dynamics | memory

Declarative memories are initially hippocampus-dependent and gradually become hippocampus-independent over time, that is, consolidated (1, 2). It is theorized that a two-stage reciprocal dialogue between the hippocampus and the cerebral cortex underlies memory consolidation (3–5). According to this model, active behavior generates experiential codes in the cortex that are transmitted to the hippocampus, which houses a labile information store. Later, during slow-wave sleep (SWS), recently acquired hippocampal information is reactivated and transmitted to the cerebral cortex, where it is integrated into a more permanent memory store (5, 6). Thus, the hippocampus and cerebral cortex are proposed to exchange roles in sending and receiving information across wake and SWS (5, 6). Importantly, this model does not imply that all signals travel from the "sender" to the "receiver." Instead, the theory proposes that high-frequency activity carries information from the sender to receiver, that is, from the cortex to hippocampus or the hippocampus to cortex, depending on the stage of memory consolidation (wake or SWS, respectively) (4). Conversely, low-frequency activity propagates from the receiver back to the sender to coordinate the transfer of high-frequency information through modulation of the sender's excitability (4, 7–9). Hence, the two-stage reciprocal dialogue model predicts that lower and higher frequency activity between the hippocampus and cortex should propagate in opposite directions across wake and SWS, as illustrated in the schematic in Fig. 1. However, such reversal has not been directly observed in humans.

We have recently analyzed temporal lags (delays) in neural signals to study the net propagation of spontaneous activity. In particular, we investigated resting-state fMRI (rs-fMRI) blood oxygen level-dependent (BOLD) signals and demonstrated directed propagation of infraslow activity (<0.1 Hz) in normal young adults (10, 11). Although rs-fMRI data are generally analyzed on the basis of zero-lag correlation topographies (e.g., functional connectivity) (12, 13), our prior work has established that the resting-state BOLD signal also exhibits a highly reproducible propagation structure in awake adults (10, 11). Moreover, in a data-driven analysis, we found that BOLD signal propagation is markedly altered in wake vs. SWS, including state-dependent reversal of propagation between subcortical structures (thalamus and striatum) and the cerebral cortex (14). On this basis, we hypothesized that the reciprocal corticohippocampal dialogue (Fig. 1) may manifest a lower frequency component in infraslow signals, whereas a higher frequency component may be found in oscillations more traditionally associated with hippocampal function (4, 15, 16).

To investigate this hypothesis, we here analyze two datasets: (*i*) combined noninvasive electroencephalography (EEG) and rs-fMRI acquired in 38 normal, young adults during wake and SWS and (*ii*) invasive electrocorticography (ECoG) data collected during wake and SWS in five patients undergoing evaluation for surgical management of epilepsy. We study infraslow propagation by examining temporal lags in corticohippocampal rs-fMRI signals as well as electrophysiological infraslow signals extracted from ECoG. Higher frequencies are examined by studying temporal lags in local field potentials (LFPs) measured using ECoG. On this basis, we investigate cortical–hippocampal propagation of both slow and fast signals in humans during wakefulness and SWS.

Results

Resting-State fMRI. We first examined infraslow signaling using rs-fMRI in 38 normal adults on the basis of prior work demonstrating

Significance

Reciprocal cortical–hippocampal signaling is widely believed to underlie consolidation of declarative memories. By investigating human fMRI and electrocorticography during both wake and slow-wave sleep (SWS), we find, first, that δ-band activity and infraslow activity propagate in opposite directions between the hippocampus and cortex. Second, both δ activity and infraslow activity reverse propagation directions between the hippocampus and the cortex across wake and SWS. These results highlight reciprocal communication between frequencies, and constitute direct evidence for the reversal of the human cortical–hippocampal dialogue across wake and SWS.

Author contributions: A.M., A.Z.S., C.D.H., E.T., H.L., E.C.L., and M.E.R. designed research; A.M., E.T., H.L., E.C.L., and M.E.R. performed research; A.M., C.D.H., and M.P. analyzed data; and A.M., A.Z.S., E.T., H.L., and M.E.R. wrote the paper.

Reviewers: E.A.B., University of Washington; G.B., New York University Neuroscience Institute; Y.N., Tel Aviv University; and O.S., Indiana University.

The authors declare no conflict of interest.

[1]To whom correspondence may be addressed. Email: mitraa@wusm.wustl.edu or marc@npg.wustl.edu.

This article contains supporting information online at www.pnas.org/lookup/suppl/doi:10.1073/pnas.1607289113/-/DCSupplemental.

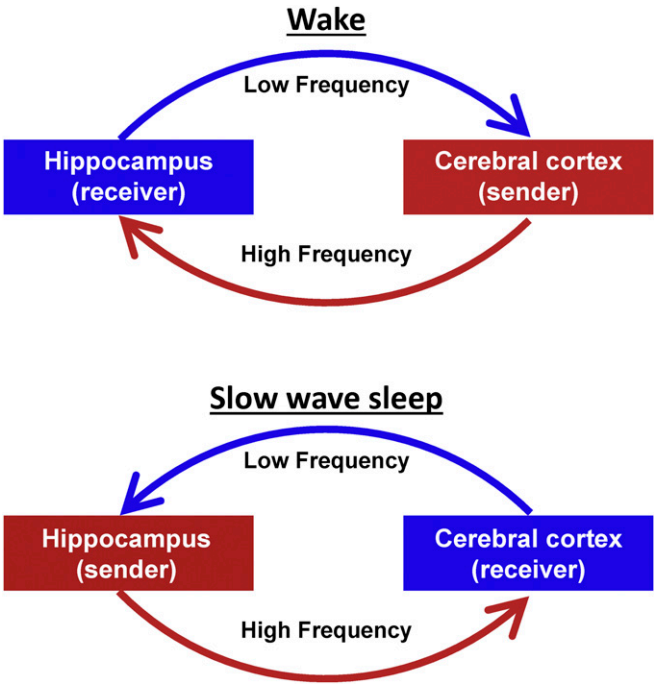

Fig. 1. Schematic representation of the two-stage reciprocal cortical–hippocampal dialogue. Information is carried by high-frequency signals. During wake and SWS, the information receiver coordinates the timing of transmissions from the sender via propagated low-frequency signals.

state-dependent reversal of BOLD signal propagation between the cortex and subcortical structures (14). As illustrated in Fig. 2, we compute temporal lags in rs-fMRI data by applying parabolic interpolation to lagged covariance curves derived over pairs of time series [this methodology has been previously described in detail (11)]. Parabolic interpolation allows the detection of temporal lags finer than the temporal sampling density of fMRI. The temporal lag between the hippocampus region of interest (ROI) and each gray matter voxel represents, on average, whether the BOLD signal in the hippocampus leads or follows the cortical voxel.

The set of all temporal lags with respect to the hippocampus, during wake and SWS, is shown in Fig. 3 in the form of a lag map. Negative lag values (cool hues) in Fig. 3 indicate voxels where activity, on average, leads the hippocampus; positive lag values (warm hues) indicate voxels where activity, on average, follows the hippocampus. The range of lags in Fig. 3, approximately ±1 s, agrees with previous findings (10). Contrasting Fig. 3 *A* and *B*, it is evident that the hippocampal lag maps are substantially altered across wake and SWS. To assess the distribution of these effects over functional systems, we computed the mean lag between the hippocampus and an array of resting state networks (RSNs) in wake and SWS (topographic network definitions are provided in *SI Appendix*, Fig. S1*A*). The results, shown in Fig. 4*A*, demonstrate that every neocortical RSN is late with respect to the hippocampus during wake. In contrast, during SWS, every RSN is early with respect to the hippocampus, with the exception of the sensory motor network (SMN). Thus, infraslow rs-fMRI activity generally propagates from the hippocampus to cerebral cortex during wake, but in the opposite direction, from the cerebral cortex to hippocampus, during SWS. This reversal in propagation is statistically significant in three networks: the visual network, the auditory network, and the default mode network (DMN).

To examine lags at a finer spatial scale, we next analyzed voxel-wise lag differences (Fig. 4*B*). Statistically significant spatial clusters are shown in Fig. 4*C*. Clusters with negative lag values (blue) in Fig. 2*C* are earlier with respect to the hippocampus during SWS compared with wake. These clusters include the posterior cingulate precuneus, parietal cortex, and medial prefrontal cortex, a constellation of regions corresponding to the DMN (17). Additional significant spatial clusters of increased earliness were found in the calcarine sulcus (visual network) and auditory cortex (auditory network).

Positive differences in lag values, indicating voxels that are later with respect to the hippocampus during SWS compared with wake, are also found in Fig. 4*B*. This effect was statistically significant in two spatial clusters (Fig. 4*C*): the paracentral lobule and parts of the right dorsal striatum (caudate nucleus and putamen). The paracentral lobule is a functional component of the supplementary motor area (SMA) (18), which belongs to the SMN. Thus, increased lateness in the paracentral lobule accounts for the exceptional status of the SMN in Fig. 4*A*. The SMA and dorsal striatum both play a major role in procedural motor learning (19). Hence, our results raise the possibility that regions integral to motor learning exhibit increased lateness with respect to the hippocampus during SWS. Indeed, a trend toward increased lateness was also observed at the voxel level in the rostral cingulate cortex (Fig. 4*B*), another area implicated in procedural motor learning (19).

In control analyses, we verified that BOLD signal amplitude in the hippocampal ROI is unchanged in wake vs. SWS (*SI Appendix*, Fig. S1*B*), as is zero-lag correlation (e.g., conventional functional connectivity) between the hippocampus and the major cortical networks (*SI Appendix*, Fig. S1*C*). Therefore, the observed shifts in BOLD signal lag cannot be attributed to loss of hippocampal signal or loss of cortical–hippocampal functional connectivity. Moreover, entorhinal cortex lag analyses yielded results nearly identical to the results obtained using the hippocampus (*SI Appendix*, Fig. S2). Therefore, the findings in Figs. 3 and 4 should be understood as applying to the hippocampal system, including entorhinal cortex.

Infraslow Electrophysiology. We have thus far examined temporal lags in rs-fMRI data. We next examined lags in infraslow activity using ECoG data collected during wake and SWS in five patients undergoing evaluation for surgical management of epilepsy (detailed information on sleep staging is provided in *SI Appendix*, *Supplemental Experimental Procedures*, and patient details are provided in *SI Appendix*, Table S1). These patients had no medial temporal lobe pathology and were grossly cognitively normal, including intact memory function. Cortical electrode coverage across subjects is illustrated in Fig. 5*A*, and the locations of electrodes in the hippocampal system in each of the five patients are shown in Fig. 5*B*.

Infraslow activity in ECoG has previously been assessed in two ways, either through infraslow LFPs (20) or infraslow fluctuations in band-limited power (BLP) (21–23). Both infraslow potentials and infraslow fluctuations in BLP exhibit temporal correlation patterns that have been shown to correspond to RSNs derived using rs-fMRI (20, 22). Owing to clinical amplifier limitations, infraslow potentials were not available in the present data; hence, we examined cortical–hippocampal lags in infraslow BLP fluctuations, parametric in carrier frequency: δ (0.5–4 Hz), θ (4–8 Hz), α (8–12 Hz), and γ (40–100 Hz). Use of infraslow BLP to assess infraslow fluctuations in electrophysiology is well established (21–24).

Accordingly, we computed lags in each subject between the hippocampal electrode and all cortical electrodes using infraslow BLP time series parametric in carrier frequency. An example of lagged covariance curves in wake and SWS, illustrated using γ BLP time series, is shown in Fig. 5*D*. To accommodate variable cortical electrode coverage across subjects, group-average lag results were computed at the network level (as in Fig. 4*A*). The most robust evidence of statistically significant reversal of lags in infra-slow BLP between the cortex and hippocampus was found in the γ BLP, as shown in Fig. 5*E*. Notably, infraslow fluctuations in γ BLP exhibited cortical–hippocampal lags closely matched to our rs-fMRI results (compare Figs. 4*A* and 5*E*). The range of γ BLP

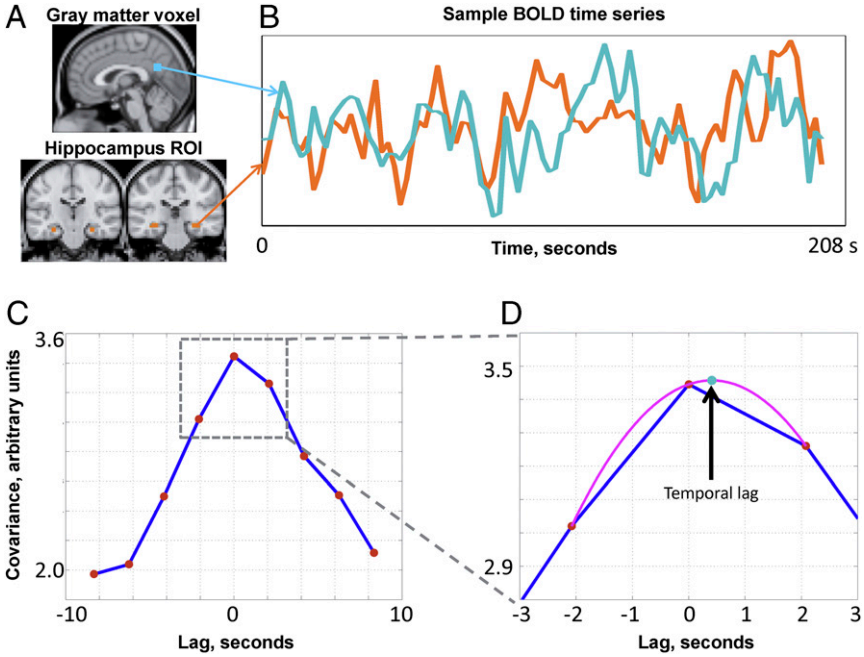

Fig. 2. Calculation of rs-fMRI temporal lags using parabolic interpolation. Lags are derived by pairwise analysis of time series derived from the hippocampus ROI and every cortical voxel. (*A*) Hippocampal ROI and a sample gray matter voxel. (*B*) Time series extracted from the regions in *A*. (*C*) Corresponding lagged cross-covariance function. The range of the plotted values is restricted to ±8.32 s, which is equivalent to plus or minus four frames (red markers) because the repetition time was 2.08 s. The lag between the time series is the value at which the absolute value of the cross-covariance function is maximal. (*D*) This extremum (arrow, teal marker) can be determined at a resolution finer than the temporal sampling density by parabolic interpolation (magenta line) through the computed values (red markers). In this example, the cortical time series is, on balance, ~0.5 s later than the hippocampal time series. Further details are provided in *Experimental Procedures* and in a study by Mitra et al. (11).

lags is similar to the range reported in Fig. 4*A* (approximately ±1 s). Moreover, with one exception, each cortical RSN was late with respect to the hippocampus during wake, whereas the reverse was true during SWS. This reversal was statistically significant in the visual network, DMN, and auditory network ($P < 0.05$, corrected). The lone exception to the finding of increased earliness in SWS was the SMN, which exhibited increased lateness with respect to the hippocampus in SWS compared with wake (Fig. 5*E*). Notably, the same SMN effect was observed in the rs-fMRI results (Fig. 4*A*).

We found no statistically significant wake vs. SWS reversal of infraslow BLP lags in the α- or θ-bands (*SI Appendix*, Fig. S3 *A* and *B*). Interestingly, one significant lag reversal was found in the visual network in δ BLP, but the direction of this lag reversal is opposite to what was observed for γ BLP (further discussion is provided in *SI Appendix*, Fig. S3 *A* and *B*). We also computed zero-lag correlations for BLP signals between the hippocampal electrode and each cortical network, and found that none of the lag changes can be attributed to statistically significant changes in correlation between wake and SWS

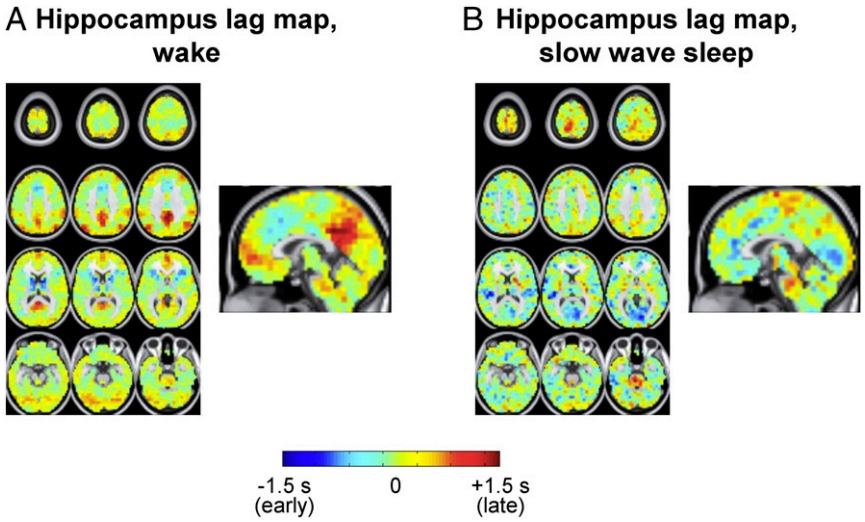

Fig. 3. Hippocampus seed-based lag maps (using the ROI in Fig. 2*A*) of infraslow rs-fMRI BOLD activity in wake (*A*) and SWS (*B*). Maps depict the mean delay between each voxel and the hippocampus seed region. Negative lag values indicate regions where activity leads the hippocampus; positive lag values indicate regions where activity follows the hippocampus. The range of lags is ~ ±1 s as shown in the color scale.

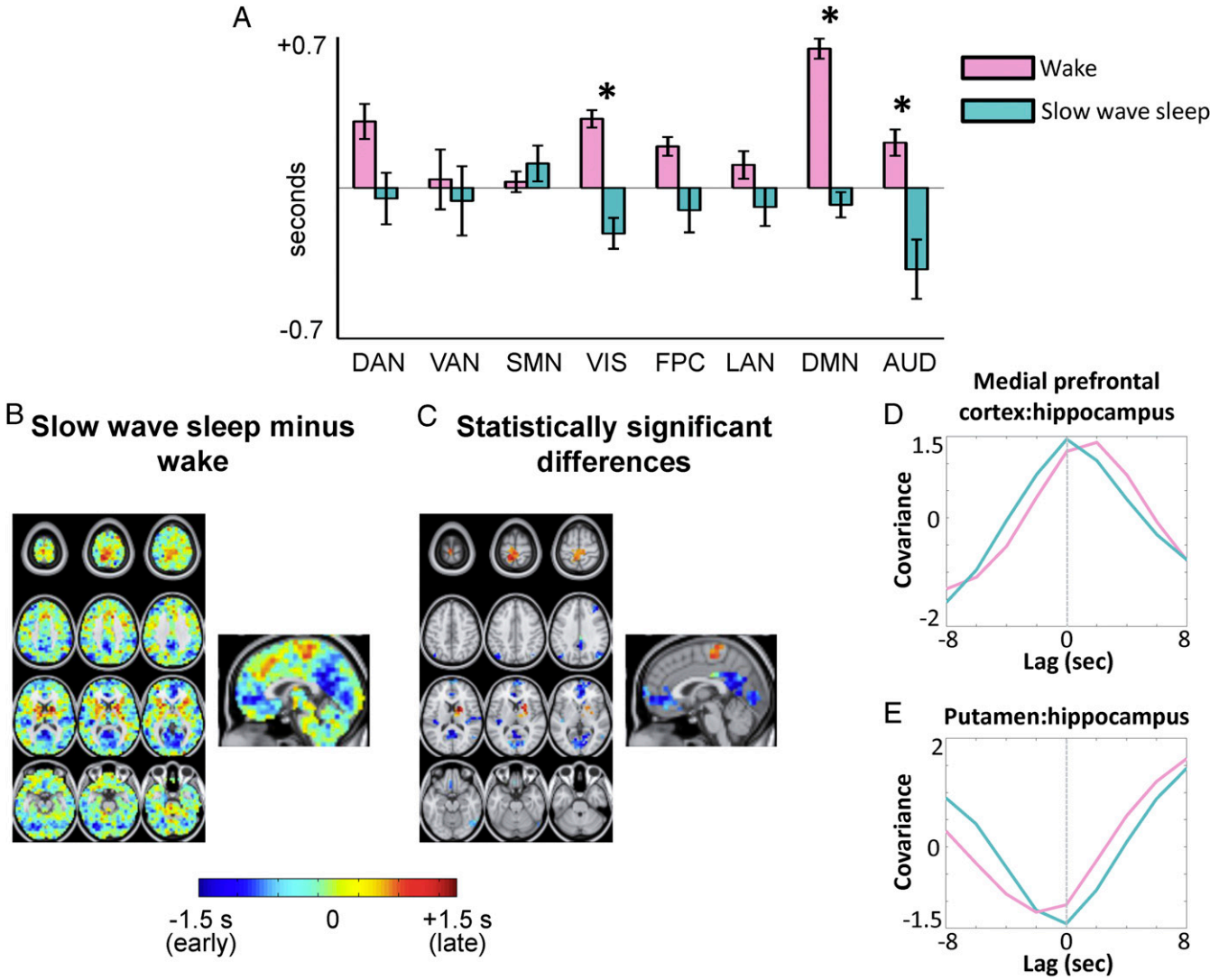

Fig. 4. Topography of wake vs. SWS rs-fMRI hippocampal lag differences. (*A*) Mean lag between the hippocampus and each of cortical eight networks during wake and SWS (network topographies are shown in *SI Appendix*, Fig. S1). Error bars represent 95% confidence intervals over subjects. (*B*) SWS minus wake hippocampus lag difference map (e.g., Fig. 3*B* minus Fig. 3*A*). (*C*) Difference map in *B*, masked for statistical significance at the spatial cluster level ($|Z| > 4.5$, $P < 0.05$ corrected). (*D* and *E*) Group-level lagged covariance curves, in wake and SWS, between the medial prefrontal cortex (mPFC) and hippocampus as well as between the putamen and hippocampus. The mPFC and putamen ROIs were derived from spatial clusters in *C*. It is evident that the mPFC shifts from "late" to "early" across wake and SWS, with respect to the hippocampus. In contrast, the putamen shifts from early to late across wake and SWS. AUD, auditory network; DAN, dorsal attention network; FPC, frontoparietal control network; LAN, language network; VAN, ventral attention network; VIS, visual network. The asterisk designates statistically significant reversal in the propagation direction (*$P < 0.05$, Bonferroni-corrected) (*Experimental Procedures*).

(*SI Appendix*, Fig. S3*C*). Stable infraslow BLP correlations across wake and SWS agree with previously reported work (21, 22). Finally, we verified that the cortical and hippocampal electrodes in each patient had power at all analyzed frequencies during both wake and SWS (*SI Appendix*, Fig. S4). Although there is more δ-band power during SWS than wake (by definition), power in δ frequencies is present during wakefulness. Moreover, as has been previously reported, γ oscillations are present during wake and SWS (25).

LFPs. The reciprocal two-stage model predicts the existence of high-frequency signals that propagate from the cerebral cortex to hippocampus during wake, and from the hippocampus to cerebral cortex during SWS (Fig. 1). To test this feature of the model, we analyzed temporal lags in LFPs. Although low-frequency LFPs, such as δ, are generally considered "slow," in the present context, they are treated as "fast" because these frequencies are at least one order of magnitude higher than the infraslow range. As before, we analyzed lags computed between the hippocampal electrode and every cortical electrode, parametric in frequency. An example is illustrated in Fig. 6*A*: The top trace shows δ-band activity in the hippocampus and a cortical electrode during wakefulness, and the bottom trace shows δ-band activity in the same electrodes in the same patient during SWS. Lagged covariance curves computed from the time series during wake and SWS are illustrated in Fig. 6*B*; in the illustrated example, it is evident that the cortex leads the hippocampus during wake (negative lag value), whereas the reverse is true during SWS (positive lag value). Group-average lag results for δ-band activity, computed at the network level, are shown in Fig. 6*C*. The range of the temporal lags in Fig. 6*C*, approximately ±50 ms, is much faster than the ∼1-s infraslow lags reported in Fig. 5*E*. In general, the cortex leads the hippocampus during wake, and the hippocampus leads the cortex during SWS. This reversal in propagation direction was statistically significant in the dorsal attention network, the visual network, and the frontoparietal control network. It is notable

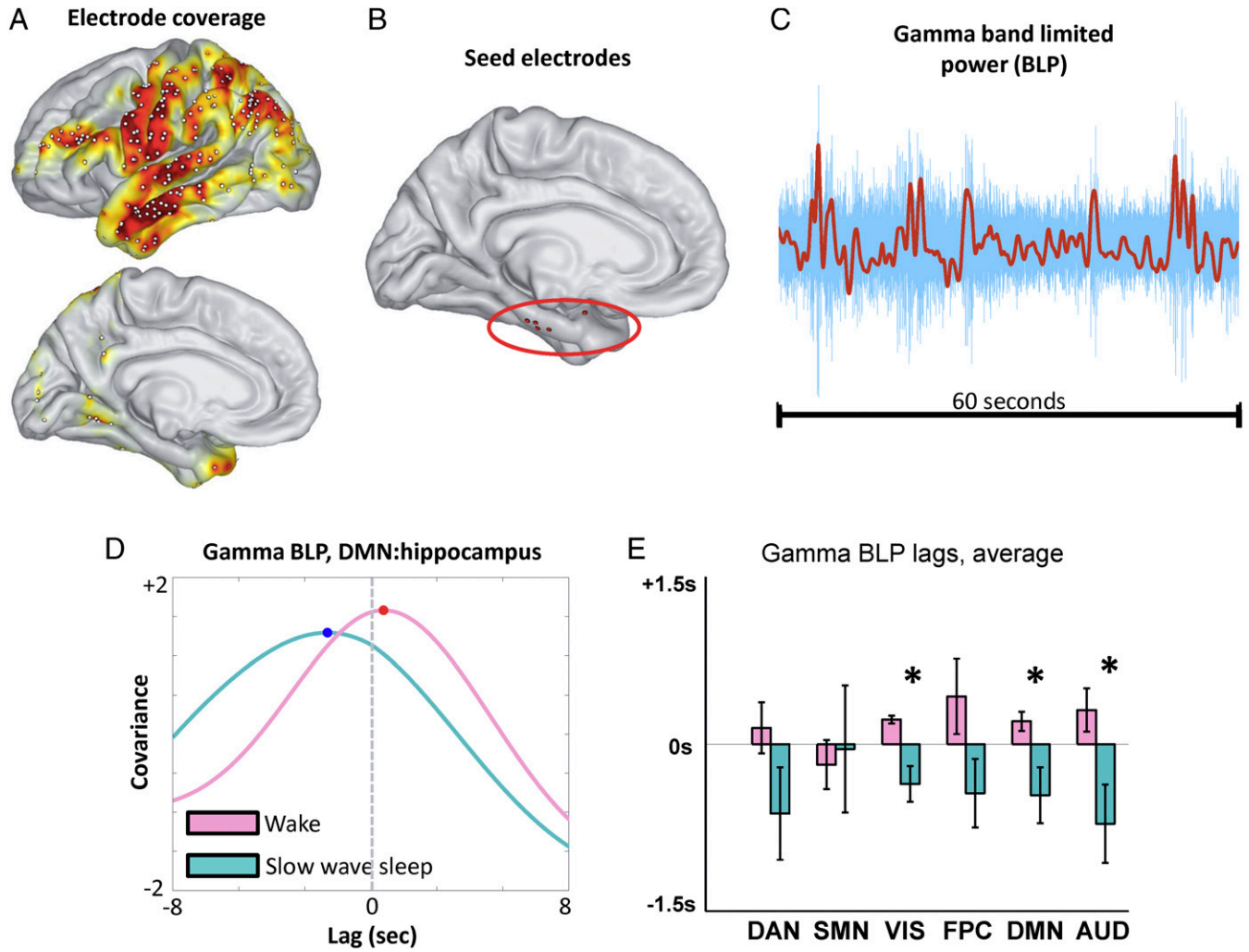

Fig. 5. Cortical–hippocampal lags in infraslow γ BLP fluctuations. (*A*) Group-level electrode coverage; the heat map indicates cross-subject coverage density. (*B*) Hippocampal system seed electrode locations for each of the five subjects. One seed electrode is more anterior than the rest; however, the results obtained in this subject are comparable to the others [patient 5 (PT5) in *SI Appendix*, Figs. S3–S5]. (*C*) Sample 60-s γ-band LFP time series (blue), along with the corresponding infraslow BLP time series (red). (*D*) Sample lagged covariance curves between two γ BLP time series (a hippocampal time series and a DMN time series) in one subject, in wake and SWS. Note that in this example, the DMN electrode is late with respect to the hippocampus during wake and early during SWS. (*E*) Group-level cortical–hippocampal lags for infraslow γ BLP. To accommodate variable cortical electrode coverage across subjects, lag results were computed at the RSN level (as in Fig. 4*A*). Note the shift from positive (late) to negative (early) temporal lags across most networks, with significant effects in VIS, DMN, and AUD. The asterisk designates statistically significant ($P < 0.05$) reversal in the propagation direction. Lag results for δ, θ, and α BLP are shown in *SI Appendix*, Fig. S3.

that the SMN exhibited the opposite effect, although this contrast was not statistically significant; that is, the net balance of propagation during wakefulness is from the hippocampus to the cortex in the SMN, and vice versa during SWS. Thus, the SMN appears as an exception in both infraslow and δ-band lag analyses.

We found no statistically significant wake vs. SWS reversal of LFP lags in the θ-, α-, or γ-bands (*SI Appendix*, Fig. S5 *A* and *B*). We also found that, at the network level, correlations in LFP activity between the hippocampus and cerebral cortex were stable across wake and SWS in all analyzed bands (*SI Appendix*, Fig. S5*C*). Thus, the changes in the direction of temporal lag found in δ activity are not attributable to changes in correlation structure.

Discussion

Summary of Present Findings. We analyzed human cortical–hippocampal signaling, as a function of wake and SWS, at multiple time scales using both rs-fMRI and ECoG. In general, we find that infraslow activity, as measured using spontaneous BOLD signals and fluctuations in γ BLP, propagates from the hippocampus to the cerebral cortex during wake, but in the opposite direction during SWS. In contrast, spontaneous δ-band LFPs measured using ECoG generally propagate from the cerebral cortex to the hippocampus during wake, and from the hippocampus to the cerebral cortex during SWS. Taken together, these results demonstrate reversal of cortical–hippocampal signaling in humans, across wake and SWS, in two distinct frequency ranges. Our findings are consistent with the two-stage reciprocal theory of corticohippocampal communication (Fig. 1), if infraslow signals are taken to represent the low-frequency component of the model and δ-band activity is viewed as the higher frequency component. These results represent a departure from rodent hippocampus studies, which associate δ/θ activity with low-frequency signaling, and γ/sharp-wave activity with higher frequency signals (26–29). We speculate that the differences may be attributable to cross-species effects (16) as well as different signaling processes captured by macro- as opposed to microelectrode recordings (30) (discussed further in *Hippocampal Delta*, below).

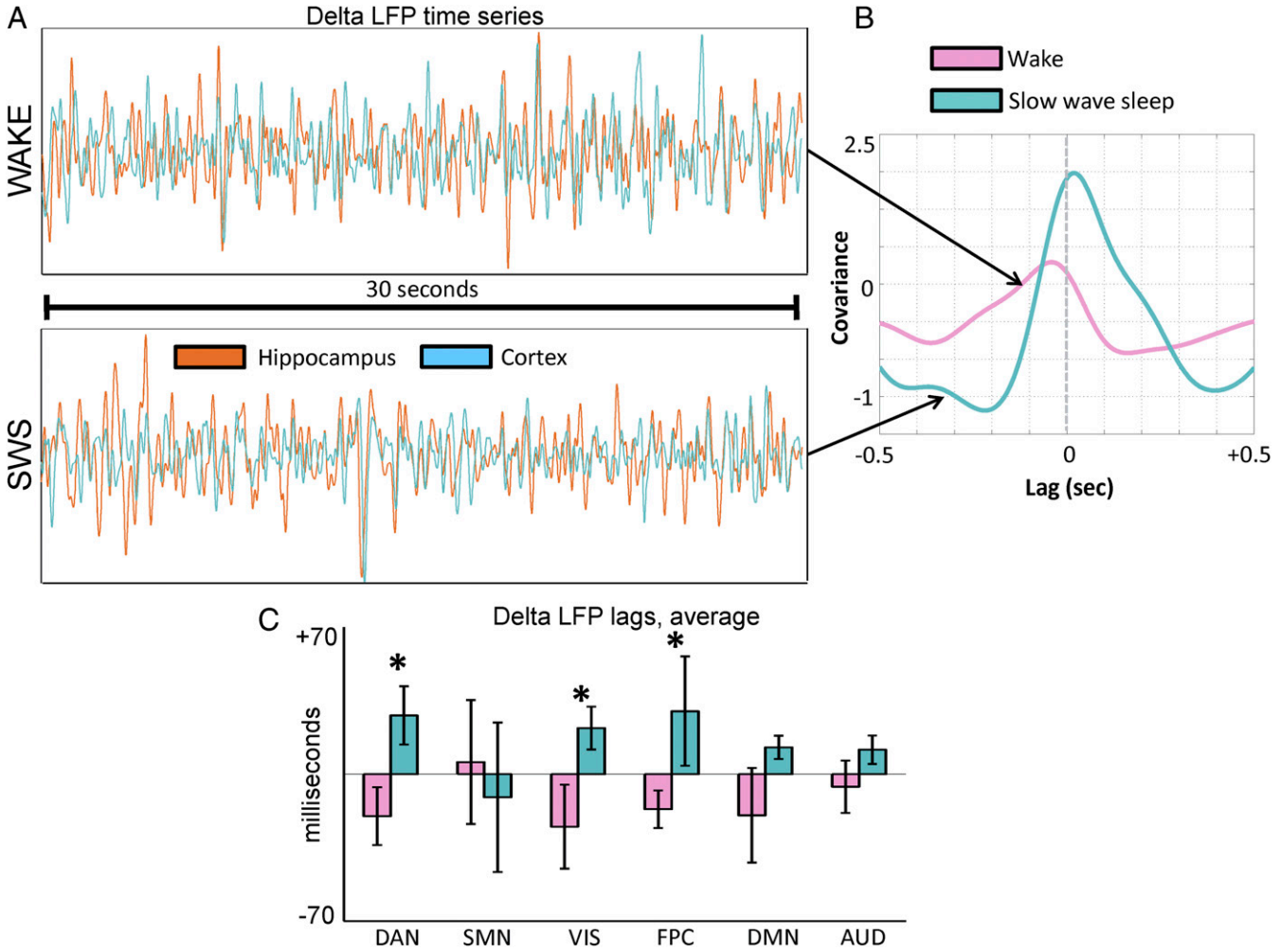

Fig. 6. Cortical–hippocampal lags in δ LFPs. (*A*) Sample 30 s of time series from the hippocampus (orange) and cortex (blue) in one subject during wake and SWS. (*B*) Lagged covariance curves corresponding to the time series in *A*. Note that in this example, the cortex is early with respect to the hippocampus during wake and late during SWS. (*C*) Group-level cortical–hippocampal lags for δ LFPs. Note the shift from negative (early) to positive (late) temporal lags across most networks, with significant effects in DAN, VIS, and FPC. The asterisk designates statistically significant ($P < 0.05$) reversal in the propagation direction. Lag results for θ, α, and γ LFPs are shown in *SI Appendix*, Fig. S5.

Our data also reveal significant exceptions to the general infraslow/δ scheme in the SMN and putamen. In these regions, the directions of the temporal lags we observed are precisely reversed from findings in the rest of the cortex, for both infralow and δ-band activity. Thus, not only is the direction of cortical–hippocampal signaling a function of wake vs. sleep and frequency but the direction of signaling also depends on the part of cortex in question (Fig. 7).

Infraslow Signaling. Our results highlight the role of infraslow activity, measured by both rs-fMRI and fluctuations in γ BLP, in the corticohippocampal dialogue. The findings suggest that the direction of infraslow propagation between the cortex and hippocampus is related to the cortical–hippocampal state (encoding vs. consolidating). The procedural memory system may be subject to a similar principle, because we have previously found reversal in propagated infraslow activity between the putamen in the cortex across wake and SWS (14).

Infraslow activity has been widely implicated in organizing brain function. First, prior work has demonstrated infraslow modulation of high-frequency corticohippocampal interactions during SWS (27). Second, it is now well known that infraslow fluctuations (assessed by rs-fMRI and electrophysiological techniques) are temporally correlated within functional systems (or resting-state networks) spanning the entire brain (20, 21). Indeed, zero-lag correlation topographies in rs-fMRI activity have been previously shown to correspond most closely to correlation topographies derived using γ BLP, as opposed to BLP fluctuations at other frequencies (21–23). Our findings extend the correspondence between rs-fMRI and infraslow fluctuations in γ BLP by demonstrating agreement in their temporal lag structure, with respect to cortical–hippocampal delays. The agreement between rs-fMRI and γ BLP suggests that large-scale coordinated infraslow fluctuations in activity, assessed by these techniques, likely correspond to spatially broad changes in cortical excitability (20, 23, 31).

In accordance with the two-stage reciprocal dialogue model, we suggest that slow, coordinated changes in excitability play a role in coordinating higher frequency information exchange between the cortex and hippocampus. It has been previously demonstrated that spontaneous infraslow activity modulates broad-band electrophysiological activity through cross-frequency, phase-amplitude coupling (31). Thus, given its broad influence over multiple temporal scales and large distances, temporal lags in infraslow activity are well suited for the coordination of systems level activity necessary for cortical–hippocampal communication. Importantly, the long temporal lags (~1 s) observed in infraslow activity indicate that these very slow frequencies do not propagate via direct axonal

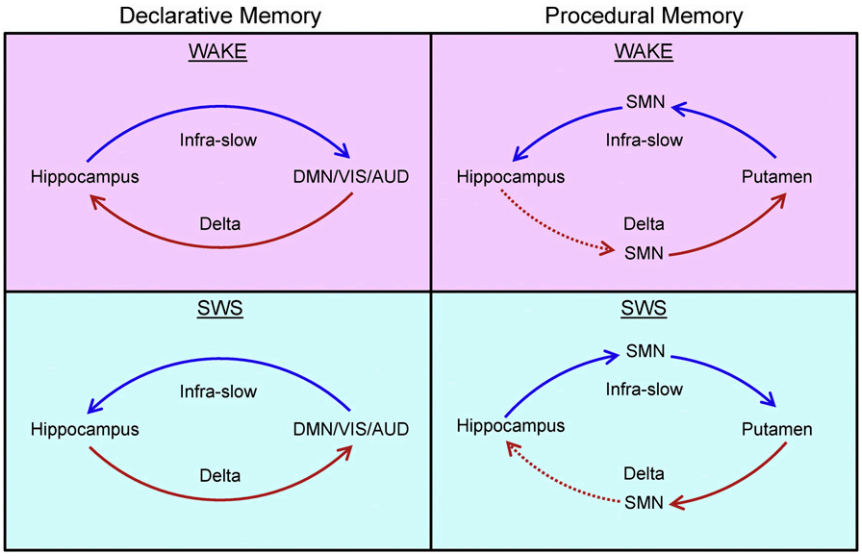

Fig. 7. Schematic of present findings. The left column depicts infraslow and δ LFP lags between the hippocampus and most of cortex, highlighting the DMN, VIS, and AUD. The temporal delays found between the hippocampus and these cortical systems agrees with the directions predicted by the two-stage reciprocal dialogue model (Fig. 1), if infraslow activity is taken to represent the low-frequency component of the model and δ LFPs represent the higher frequency component. However, the right column demonstrates that precisely the opposite lags are found when considering the putamen and the SMN with respect to the hippocampus. Dotted red lines designate temporal lags implied, but not directly observed, by mirrored dissociation between systems. We hypothesize that the temporal lags depicted in the left and right columns may represent the parallel functions of the declarative and procedural memory systems, respectively. As depicted in the right column, our results suggest that the hippocampus is in an ongoing dialogue with the procedural memory system.

transmission; instead, we hypothesize that infraslow signals travel at the population level to act as a slow feedback signal to regulate higher frequency activity.

Our study does not address the mechanisms that cause the direction of propagated infraslow activity between the hippocampus and cortex to reverse. However, prior evidence suggests that the differences in neuromodulator tone between wake and SWS (32), especially cholinergic input (7, 33), play a role in altering patterns of intrinsic activity. Specifically, the reduction of cholinergic tone during SWS (33) may differentially alter the excitatory/inhibitory balance in different parts of the brain (34). Regionally variable differences in excitatory tone could underlie reversals in the net propagation of activity. The physiology underlying infraslow propagation over hundreds to thousands of milliseconds is also presently unknown. This mechanistic uncertainty extends to propagation of ∼1-Hz activity over hundreds of milliseconds, where prior work has implicated factors ranging from purinergic signaling to the balance in excitatory and inhibitory activity (7, 35). Future work is required to resolve these questions.

Hippocampal Delta. We find that, on balance, spontaneous δ LFPs propagate from the cerebral cortex to the hippocampus during wakefulness, and from the hippocampus to the cerebral cortex during SWS. These results, in the context of the two-stage reciprocal dialogue model, suggest that δ-band activity plays a role in human cortical–hippocampal information exchange in both wake and sleep. Although hippocampal function has been traditionally associated with θ (4–8 Hz) -band activity on the basis of rodent studies (28, 36), recent work has shown that memory-related activity in the primate (including human) hippocampus manifests also in the δ (0.5–4 Hz) range (16, 37–41). Human ECoG studies have shown that δ LFP activity propagates from the cortex to hippocampus with a delay of ∼30 ms during recall tasks (39), in agreement with the delay time and direction observed in our awake data (Fig. 6*B*). Furthermore, δ power in the human hippocampus increases during SWS following a memory task, and the degree of this increase is correlated with postsleep memory recall (37), suggesting a role for hippocampal δ in memory consolidation during SWS. To the best of our knowledge, phase delays in δ LFPs between the hippocampus and cortex have not been previously studied in human SWS. However, our finding of signaling from the hippocampus to cerebral cortex in SWS is consistent with δ activity facilitating consolidation by transfer of information from the hippocampus to cortex.

The propagation of δ LFPs from the hippocampus to much of the cortex during SWS may appear, at first glance, to contradict prior work, which has demonstrated propagation of slow waves from the cortex to hippocampus (9, 42). However, much of the prior work examining slow-wave (or up/down state) propagation has used motor cortex recordings to examine the cortico-hippocampal relationship (9, 42). In agreement with these studies, we find that δ LFPs in the motor cortex propagate to the hippocampus during SWS (Fig. 5*E*). Thus, in evaluating cortical–hippocampal propagation of activity, cortical location is a critical factor, as further discussed in *Network Specificity*. In this regard, a present limitation is the lack of medial electrode coverage (Fig. 5*A*); it is quite possible that these medial structures have a different lag relation to the hippocampus, in δ LFPs, than the lateral regions we measured. Finally, it is important to note that δ LFPs represent a broader set of neural processes than slow waves (43). Our focus on contrasting wake vs. SWS informed the present focus on δ LFPs rather than slow-wave events, but differences between these phenomena may drive some differences in cortico–hippocampal relations (further discussion is provided in *SI Appendix, Supplemental Experimental Procedures*).

We did not observe consistent cortical–hippocampal temporal lags in θ, α, or γ LFPs. However, this negative finding does not mean that activity in these frequencies does not play an essential role in cortical–hippocampal communication. Our temporal lags analysis detects biases in the direction of signaling; thus, strongly reciprocal signaling, which may be equally important for cortical–hippocampal communication, may not produce a clear lag direction. Moreover, our LFP data are acquired on the basis of ECoG electrodes on the surface of the brain. These electrodes do not provide the cortical laminar specificity that has been essential for detecting directed α- and γ-band activity in other parts of the brain (30, 44). Finally, it is important to note the caveat that the present electrophysiological recordings are obtained in patients with epilepsy.

Hence, it is possible that the findings reported here may not generalize to normal human physiology. The agreement between the results obtained using rs-fMRI in normal subjects and γ BLP in patients with epilepsy is a good control with respect to infraslow signaling, but ethical considerations prevent any similar comparison with normal participants with respect to LFP data.

Network Specificity. In general, infraslow activity (rs-fMRI and γ BLP) propagates from the hippocampus to the cerebral cortex during wakefulness, and in the reverse direction during SWS. δ LFP activity between the hippocampus and cortex generally travels in the opposite direction as infraslow activity during wake and SWS. These reversals are especially prominent in the DMN, the visual network, and the auditory network. A prominent DMN effect is significant, given the emerging work associating the ongoing function of this network with declarative memory processes both during waking recall (22, 45) and during offline consolidation (46). Functional signaling between the hippocampus and the DMN is also consistent with the robust anatomical connections between these systems (47). Therefore, our findings add to growing evidence that the ongoing activity in the DMN is intimately related to declarative memory function.

Prominent lag reversals in the visual and auditory networks suggest the key role of sensory systems in both encoding and consolidating declarative memories. Previous work has shown that sensory information is conveyed to the hippocampus during wakefulness (3, 5, 36) and that neurons in both the auditory and visual cortices engage in coordinated high-frequency replay with the hippocampus during SWS (48–50). Temporal lag reversals between the hippocampus and visual/auditory cortices may reflect systems-level manifestations of these processes.

Propagation between the SMN, including the putamen (as measured in rs-fMRI), and the hippocampus occurs in the opposite direction with respect to the rest of the cortex, at infraslow and δ frequencies, during wake and SWS. These results are consistent with prior work that has demonstrated a fundamental dissociation between the declarative memory system, which is hippocampus-dependent, and the procedural memory system, which depends on the striatum and supports motor learning and habitual behavior (32, 51–54) (Fig. 7). However, although the direction of propagation dissociates the procedural memory system from other parts of the brain, we also find evidence of signaling between the elements of the procedural system (SMN and putamen) and the hippocampus. Thus, our data suggest that in addition to functional dissociation, there is ongoing communication between the declarative and procedural memory systems, in which the hippocampus appears to play an important role. This view is consistent with prior work demonstrating coordination between the declarative and procedural memory systems (54).

Conclusion

Analysis of human spontaneous brain activity reveals direct evidence for reciprocal cortical–hippocampal communication across lower (infraslow rs-fMRI and γ BLP) and higher (δ LFP) frequency signals. As predicted by the two-stage model of declarative memory consolidation, the direction of propagation in both the slower (infraslow) and faster (δ) signals reverses direction in SWS vs. wake. However, the direction of hippocampal signaling with sensory motor areas differs compared with the rest of the brain. Future work is required to determine the behavioral role of this propagated activity, as well as to investigate how these frequencies relate to other cortical and hippocampal rhythms.

Experimental Procedures

EEG-fMRI Acquisition and Artifact Correction. Acquisition parameters and details for these data have been previously published (55). The fMRI was acquired using a 3T scanner (Siemens Trio) with optimized polysomnographic settings (1,505 vol of T2*-weighted echo planar images, repetition time/echo time = 2,080 ms/30 ms, matrix = 64 × 64, voxel size = 3 × 3 × 2 mm^3, distance factor = 50%, field of view = 192 mm^2). Thirty EEG channels were simultaneously recorded using a modified cap (EASYCAP) with FCz as a reference (sampling rate = 5 kHz, low-pass filter = 250 Hz, high-pass filter = 0.016 Hz). MRI and pulse artifact correction were performed based on the average artifact subtraction method (56) as implemented in BrainVision Analyzer 2 (Brain Products), followed by independent components analysis (ICA)-based rejection of residual artifact components (CBC parameters; Vision Analyzer). EEG sleep staging was done by an expert according to the American Academy of Sleep Medicine criteria (57).

fMRI Subjects. Sixty-three nonsleep-deprived subjects were scanned in the evening (starting at ∼8:00 PM). Written informed consent was obtained from all subjects whose data were analyzed in this study, and data collection for this study was approved by the Goethe University Ethics Committee. Hypnograms were inspected to identify epochs of contiguous sleep stages lasting at least 5 min (150 volumes). These criteria yielded 38 subjects contributing to the present analyses. Included are 70 epochs of wakefulness and 38 epochs of N3 sleep (SWS). Detailed sleep architectures of each participant have been previously published (55).

ECoG Subjects. All participants were patients at Barnes Jewish Hospital or St. Louis Children's Hospital with drug-resistant epilepsy undergoing ECoG monitoring to localize seizure foci. All participants provided informed consent with oversight by the local Institutional Review Board at the Washington University School of Medicine in accordance with the NIH guidelines and the ethical standards of the Declaration of Helsinki. Participants were selected from a large ECoG database in which least 4 d of clinical ECoG recordings as well as preoperative structural MRI and fMRI and postimplant X-ray computed tomography images were acquired (n = 25). Five subjects passed stringent electrophysiological and spatial coverage criteria (*SI Appendix, Supplemental Experimental Procedures*) for inclusion in the study. We only analyzed data from patients who did not show any sign of medial temporal lobe pathology, were grossly cognitively normal by clinical neurological assessment, showed no signs of memory impairment, and had a combined intelligence quotient >80 as assessed by the *Wechsler Adult Intelligence Scale—Fourth Edition* (58). Furthermore, four of the five subjects in the present analysis were not on any medications during the ECoG recording period. Individual subject profiles are provided in *SI Appendix*, Table S1.

Epochs of wakefulness and sleep in the patients were identified behaviorally with video records. Periods of SWS during sleep were identified electrophysiologically on the basis of δ power in ECoG electrodes. δ Power was assessed using ECoG electrodes as opposed to traditional scalp EEG because, as noted by prior studies, the postsurgical condition of the skull precludes collection of usable EEG/polysomnography data (59). Thus, following previously established practice (20, 59), we classified sustained periods (≥5 min) of δ power (>20% power in the 0.5- to 2-Hz range) in ECoG electrodes during behaviorally identified sleep as SWS (20, 57). We only analyzed SWS epochs lasting a minimum of 5 min to match the fMRI analysis.

Statistical Analysis. Statistical significance of wake vs. SWS differences in lag maps (Fig. 4) was assessed on a cluster-wise basis using threshold-extent criteria computed by extensive permutation resampling (60, 61). Statistical significance in group-level lag reversals (Figs. 4–6) is computed using a one-sample t test, where statistically significant reversals are inferred only when mean lag values are significantly different from zero, and in opposite directions, across wake and SWS. P values in Fig. 4 were Bonferroni-corrected for eight comparisons; P values in Figs. 5 and 6 were Bonferroni-corrected for 24 comparisons (six networks × four frequency bands).

Details regarding preprocessing of fMRI and ECoG data, as well as further explanation of lags computations, are found in *SI Appendix, Supplemental Experimental Procedures*.

ACKNOWLEDGMENTS. We thank Gyorgy Buzsaki, Manu Goyal, and Tyler Blazey for helpful discussion. This work was supported by NIH Grants NS080675 (to M.E.R. and A.Z.S.), P30NS048056 (to A.Z.S.), R01MH096482-01 (to E.C.L.), F30MH099877-02 (to C.D.H.), and F30MH106253-02 (to A.M.); the Bundesministerium für Bildung und Forschung (Grant 01EV0703); and the Landes-Offensive zur Entwicklung wissenschaftlich ökonomischer Exzellenz (LOEWE) Neuronale Koordination Forschungsschwerpunkt Frankfurt.

1. Scoville WB, Milner B (1957) Loss of recent memory after bilateral hippocampal lesions. *J Neurol Neurosurg Psychiatry* 20(1):11–21.

2. Squire LR, Alvarez P (1995) Retrograde amnesia and memory consolidation: A neurobiological perspective. *Curr Opin Neurobiol* 5(2):169–177.

3. Buzsáki G (1989) Two-stage model of memory trace formation: A role for "noisy" brain states. *Neuroscience* 31(3):551–570.
4. Sirota A, et al. (2008) Entrainment of neocortical neurons and gamma oscillations by the hippocampal theta rhythm. *Neuron* 60(4):683–697.
5. Buzsáki G (1996) The hippocampo-neocortical dialogue. *Cereb Cortex* 6(2):81–92.
6. McNaughton BL, et al. (2003) Off-line reprocessing of recent memory and its role in memory consolidation: A progress report. *Sleep and Brain Plasticity*, eds Maquet P, Smith C, Stickgold R (University Press Scholarship Online, New York), pp 215–249.
7. Hahn TT, McFarland JM, Berberich S, Sakmann B, Mehta MR (2012) Spontaneous persistent activity in entorhinal cortex modulates cortico-hippocampal interaction in vivo. *Nat Neurosci* 15(11):1531–1538.
8. Wilson MA, McNaughton BL (1994) Reactivation of hippocampal ensemble memories during sleep. *Science* 265(5172):676–679.
9. Isomura Y, et al. (2006) Integration and segregation of activity in entorhinal-hippocampal subregions by neocortical slow oscillations. *Neuron* 52(5):871–882.
10. Mitra A, Snyder AZ, Blazey T, Raichle ME (2015) Lag threads organize the brain's intrinsic activity. *Proc Natl Acad Sci USA* 112(17):E2235–E2244.
11. Mitra A, Snyder AZ, Hacker CD, Raichle ME (2014) Lag structure in resting-state fMRI. *J Neurophysiol* 111(11):2374–2391.
12. Biswal B, Yetkin FZ, Haughton VM, Hyde JS (1995) Functional connectivity in the motor cortex of resting human brain using echo-planar MRI. *Magn Reson Med* 34(4): 537–541.
13. Fox MD, Raichle ME (2007) Spontaneous fluctuations in brain activity observed with functional magnetic resonance imaging. *Nat Rev Neurosci* 8(9):700–711.
14. Mitra A, Snyder AZ, Tagliazucchi E, Laufs H, Raichle ME (2015) Propagated infra-slow intrinsic brain activity reorganizes across wake and slow wave sleep. *eLife* 4:4.
15. Buzsáki G, Logothetis N, Singer W (2013) Scaling brain size, keeping timing: evolutionary preservation of brain rhythms. *Neuron* 80(3):751–764.
16. Jacobs J (2013) Hippocampal theta oscillations are slower in humans than in rodents: Implications for models of spatial navigation and memory. *Philos Trans R Soc Lond B Biol Sci* 369(1635):20130304.
17. Raichle ME, et al. (2001) A default mode of brain function. *Proc Natl Acad Sci USA* 98(2):676–682.
18. Lim SH, et al. (1994) Functional anatomy of the human supplementary sensorimotor area: results of extraoperative electrical stimulation. *Electroencephalogr Clin Neurophysiol* 91(3):179–193.
19. Halsband U, Lange RK (2006) Motor learning in man: A review of functional and clinical studies. *J Physiol Paris* 99(4-6):414–424.
20. He BJ, Snyder AZ, Zempel JM, Smyth MD, Raichle ME (2008) Electrophysiological correlates of the brain's intrinsic large-scale functional architecture. *Proc Natl Acad Sci USA* 105(41):16039–16044.
21. Nir Y, et al. (2008) Interhemispheric correlations of slow spontaneous neuronal fluctuations revealed in human sensory cortex. *Nat Neurosci* 11(9):1100–1108.
22. Foster BL, Rangarajan V, Shirer WR, Parvizi J (2015) Intrinsic and task-dependent coupling of neuronal population activity in human parietal cortex. *Neuron* 86(2): 578–590.
23. Leopold DA, Murayama Y, Logothetis NK (2003) Very slow activity fluctuations in monkey visual cortex: Implications for functional brain imaging. *Cereb Cortex* 13(4): 422–433.
24. Liu X, Yanagawa T, Leopold DA, Fujii N, Duyn JH (2015) Robust long-range coordination of spontaneous neural activity in waking, sleep and anesthesia. *Cereb Cortex* 25(9):2929–2938.
25. Le Van Quyen M, et al. (2010) Large-scale microelectrode recordings of high-frequency gamma oscillations in human cortex during sleep. *J Neurosci* 30(23):7770–7782.
26. Sirota A, Buzsáki G (2005) Interaction between neocortical and hippocampal networks via slow oscillations. *Thalamus Relat Syst* 3(4):245–259.
27. Sirota A, Csicsvari J, Buhl D, Buzsáki G (2003) Communication between neocortex and hippocampus during sleep in rodents. *Proc Natl Acad Sci USA* 100(4):2065–2069.
28. Buzsáki G (2002) Theta oscillations in the hippocampus. *Neuron* 33(3):325–340.
29. Roumis DK, Frank LM (2015) Hippocampal sharp-wave ripples in waking and sleeping states. *Curr Opin Neurobiol* 35:6–12.
30. Buffalo EA, Fries P, Landman R, Buschman TJ, Desimone R (2011) Laminar differences in gamma and alpha coherence in the ventral stream. *Proc Natl Acad Sci USA* 108(27): 11262–11267.
31. Monto S, Palva S, Voipio J, Palva JM (2008) Very slow EEG fluctuations predict the dynamics of stimulus detection and oscillation amplitudes in humans. *J Neurosci* 28(33):8268–8272.
32. Stickgold R (2005) Sleep-dependent memory consolidation. *Nature* 437(7063):1272–1278.
33. Hasselmo ME (1999) Neuromodulation: Acetylcholine and memory consolidation. *Trends Cogn Sci* 3(9):351–359.
34. Buzsáki G, Kaila K, Raichle M (2007) Inhibition and brain work. *Neuron* 56(5):771–783.
35. Poskanzer KE, Yuste R (2011) Astrocytic regulation of cortical UP states. *Proc Natl Acad Sci USA* 108(45):18453–18458.
36. Battaglia FP, Benchenane K, Sirota A, Pennartz CM, Wiener SI (2011) The hippocampus: Hub of brain network communication for memory. *Trends Cogn Sci* 15(7): 310–318.
37. Moroni F, et al. (2014) Hippocampal slow EEG frequencies during NREM sleep are involved in spatial memory consolidation in humans. *Hippocampus* 24(10):1157–1168.
38. Moroni F, et al. (2012) Slow EEG rhythms and inter-hemispheric synchronization across sleep and wakefulness in the human hippocampus. *Neuroimage* 60(1):497–504.
39. Lega BC, Jacobs J, Kahana M (2012) Human hippocampal theta oscillations and the formation of episodic memories. *Hippocampus* 22(4):748–761.
40. Watrous AJ, Fried I, Ekstrom AD (2011) Behavioral correlates of human hippocampal delta and theta oscillations during navigation. *J Neurophysiol* 105(4):1747–1755.
41. Arnolds DE, Lopes da Silva FH, Aitink JW, Kamp A, Boeijinga P (1980) The spectral properties of hippocampal EEG related to behaviour in man. *Electroencephalogr Clin Neurophysiol* 50(3-4):324–328.
42. Nir Y, et al. (2011) Regional slow waves and spindles in human sleep. *Neuron* 70(1): 153–169.
43. Amzica F, Steriade M (1998) Electrophysiological correlates of sleep delta waves. *Electroencephalogr Clin Neurophysiol* 107(2):69–83.
44. van Kerkoerle T, et al. (2014) Alpha and gamma oscillations characterize feedback and feedforward processing in monkey visual cortex. *Proc Natl Acad Sci USA* 111(40): 14332–14341.
45. Stevens WD, Buckner RL, Schacter DL (2010) Correlated low-frequency BOLD fluctuations in the resting human brain are modulated by recent experience in category-preferential visual regions. *Cereb Cortex* 20(8):1997–2006.
46. Kaplan R, et al. (2016) Hippocampal sharp-wave ripples influence selective activation of the default mode network. *Curr Biol* 26(5):686–691.
47. Lavenex P, Amaral DG (2000) Hippocampal-neocortical interaction: A hierarchy of associativity. *Hippocampus* 10(4):420–430.
48. Ji D, Wilson MA (2007) Coordinated memory replay in the visual cortex and hippocampus during sleep. *Nat Neurosci* 10(1):100–107.
49. Bendor D, Wilson MA (2012) Biasing the content of hippocampal replay during sleep. *Nat Neurosci* 15(10):1439–1444.
50. Haggerty DC, Ji D (2015) Activities of visual cortical and hippocampal neurons co-fluctuate in freely moving rats during spatial behavior. *eLife* 4:e08902.
51. Knowlton BJ, Mangels JA, Squire LR (1996) A neostriatal habit learning system in humans. *Science* 273(5280):1399–1402.
52. Eichenbaum H, Otto T, Cohen NJ (1992) The hippocampus—What does it do? *Behav Neural Biol* 57(1):2–36.
53. Logothetis NK, et al. (2012) Hippocampal-cortical interaction during periods of subcortical silence. *Nature* 491(7425):547–553.
54. DeCoteau WE, et al. (2007) Learning-related coordination of striatal and hippocampal theta rhythms during acquisition of a procedural maze task. *Proc Natl Acad Sci USA* 104(13):5644–5649.
55. Tagliazucchi E, et al. (2013) Breakdown of long-range temporal dependence in default mode and attention networks during deep sleep. *Proc Natl Acad Sci USA* 110(38):15419–15424.
56. Allen PJ, Polizzi G, Krakow K, Fish DR, Lemieux L (1998) Identification of EEG events in the MR scanner: The problem of pulse artifact and a method for its subtraction. *Neuroimage* 8(3):229–239.
57. Iber C (2007) *The AASM Manual for the Scoring of Sleep and Associated Events: Rules, Terminology and Technical Specifications* (American Academy of Sleep Medicine, Darien, IL).
58. Wechsler D (2008) *Wechsler Adult Intelligence Scale—Fourth Edition* (Pearson, San Antonio, TX).
59. Hangya B, et al. (2011) Complex propagation patterns characterize human cortical activity during slow-wave sleep. *J Neurosci* 31(24):8770–8779.
60. Hayasaka S, Nichols TE (2003) Validating cluster size inference: Random field and permutation methods. *Neuroimage* 20(4):2343–2356.
61. Hacker CD, Perlmutter JS, Criswell SR, Ances BM, Snyder AZ (2012) Resting state functional connectivity of the striatum in Parkinson's disease. *Brain* 135(Pt 12): 3699–3711.

Supplementary Materials

Supplemental Experimental Procedures

fMRI preprocessing:

fMRI preprocessing was as described in (Mitra et al., 2015b). Briefly, this included compensation for slice-dependent time shifts, elimination of systematic odd-even slice intensity differences due to interleaved acquisition, and rigid body correction of head movement within and across runs. Atlas transformation was achieved by composition of affine transforms connecting the fMRI volumes with the T2-weighted and T1-weighted structural images. Additional preprocessing in preparation for lags analysis included spatial smoothing (6 mm full width at half maximum (FWHM) Gaussian blur in each direction), voxel-wise removal of linear trends over each fMRI run, and temporal low-pass filtering retaining frequencies below 0.1 Hz. Spurious variance was reduced by regression of nuisance waveforms derived from head motion correction and timeseries extracted from regions (of "non-interest") in white matter and CSF as well the BOLD timeseries averaged over the brain (Fox et al., 2009). Frame censoring was computed at a threshold of 0.5% root mean square frame-to-frame intensity change (Power et al., 2012). Epochs containing fewer than 10 contiguous frames were excluded. These criteria removed 5.3 ± 0.9% of frames per individual during wake and 5.8 ± 0.7% during slow wave sleep. There was no statistically significant difference in the amount of frame censoring by state. Hippocampus (Main Text Fig. 2) and entorhinal cortex (Supplemental Fig. S2) ROIs were defined according to FreeSurfer segmentation of gray matter. The spatial resolution of fMRI at 3T does not permit analysis of individual hippocampal sub-fields.

ECoG Electrode Registration:

After electrode implantation, a post-operative CT image was registered (6-parameter rigid body) to the pre-operative T1 image. Post-implantation, ECoG electrodes generally are displaced downwards relative to the pre-operative brain surface owing to traction generated by dural over-sewing. To correct this displacement, electrodes were projected to a highly smoothed pial surface (a modified FreeSurfer segmentation) using normal vectors computed from grid and strip geometry. Following this correction, total electrode localization error was estimated as ~2 mm, similar to Hermes et al (Hermes et al., 2010). Only subjects with electrode coverage in the hippocampal system (hippocampal, entorhinal cortex) were considered for further analysis.

ECoG Data Acquisition and Preprocessing:

Implanted electrodes (platinum, 4 mm, 2.3 mm exposed, PMT corporation) were 8x8 or 6x8 grids (with 10 mm spacing) and strips (1x4, 1x6, or 1x8), placed subdurally facing the cortical surface. A separate strip facing the skull served as ground and reference for

the amplifier (Proamp, Lamont Medical Inc). The amplifier high-pass filtered recordings at 0.5 Hz. Data were screened for channels with excessive noise and epochs with excessive environmental noise across all channels. Channels exhibiting inter-ictal activity also were excluded. ECoG signals were referenced to a common average. A notch-filter was applied to remove 60 Hz noise. A de-spiking function, $f_{(x)} = A * \mathrm{atan}(\frac{x}{A})$, where *A* is 5 standard deviations of the signal, was applied to attenuate transient artifacts from medical devices (e.g., IV pumps). Data were further inspected for artifact in the time-frequency domain. Ictal events were identified by clinical staff. ECoG data recorded up to 2 hours following ictal events were excluded. Additional preprocessing in preparation for infra-slow lags analysis entailed temporal censoring of epochs likely contaminated by artifact. Censoring was applied using BLP frequency bands, in each subject during each state (wake and SWS; see below), by computing pair-wise correlation between the seed-electrode and every other electrode over each continuous run using a sliding window (5 minute windows, 1 minute overlap). On this basis, we computed a median value and standard deviation for the correlation across each electrode pair. 1 minute epochs in which the pair-wise correlation of all electrodes exceeded 4 standard deviations from the median of that run were excluded from further analysis. In both wake and SWS, only temporally contiguous epochs of ≥ 5 minutes were analyzed for temporal lags (see table S1). These same epochs were analyzed for LFP lags. Finally, only electrodes exhibiting a median correlation (Pearson r) $\geq |.05|$ with the seed electrode were used for cross-correlation based lags analysis (see table S1).

Sleep/wake epochs were defined behaviorally with video records and electrophysiologically on the basis of delta power in ECoG electrodes. Delta power was assessed using ECoG electrodes as opposed to traditional scalp EEG because, as noted by prior studies, the post-surgical condition of the skull precludes collection of usable EEG data (Hangya et al., 2011). Thus, following previously established practice (Hangya et al., 2011; He et al., 2008), we classified sustained periods (≥5 minutes) of delta power (> 20% power in the 0.5-2 Hz range) in ECoG electrodes during behaviorally identified sleep as slow wave sleep (SWS) (He et al., 2008; Iber, 2007). Spectral characteristics of electrodes during wake and SWS are shown in Supplemental Figure S4. The present ECoG analyses include only awake ECoG recordings at least 30 minutes separated from behaviorally identified sleep (on the basis of video recordings) and SWS ECoG recordings electrophysiologically identified as SWS. The correlation structure of the censored data, across carrier frequencies, was not statistically different in wake vs. SWS, as has been previously reported (Foster et al., 2015; He et al., 2008), with the exception of altered visual network correlation in theta BLP (Supplemental Fig. S3C). ECoG signals were decomposed into frequency components by zero-phase digital filtering using a 2nd order Butterworth filter in the

forward and reverse directions (effectively, 4th order). To compute BLP, filtered signals were squared to produce instantaneous power, then further band-pass filtered into the infra-slow range (<0.1 Hz, as illustrated in Main Text Fig. 4C).

Computation of lag between time series:

Our method for computing lags between rs-fMRI time series has been previously published (Mitra et al., 2014b). Conventional seed-based correlation analysis involves computation of the Pearson correlation, r, between the time series, $x_1(t)$, extracted from a seed region, and a second time series, $x_2(t)$, extracted from some other locus (single voxel or region of interest). Thus,

$$r_{x_1x_2} = \frac{1}{\sigma_{x_1}\sigma_{x_2}}\frac{1}{T}\int x_1(t)\cdot x_2(t)dt, \qquad \text{[E1]}$$

where σ_{x_1} and σ_{x_2} are the temporal standard deviations of signals x_1 and x_2, and T is the interval of integration. Here, we generalize the assumption of exact temporal synchrony and compute lagged cross-covariance functions. Thus,

$$C_{x_1x_2}(\tau) = \frac{1}{T}\int x_1(t+\tau)\cdot x_2(t)dt, \qquad \text{[E2]}$$

where τ is the lag (in units of time). The value of τ at which $C_{x_1x_2}(\tau)$ exhibits an extremum defines the temporal lag (equivalently, delay) between signals x_1 and x_2 (Konig, 1994). In rs-fMRI data, we determine the extremum abscissa and ordinate using parabolic interpolation (Mitra et al., 2014b). In ECoG data, given high temporal sampling density (512 Hz), we determine the extremum abscissa and ordinate by empirical peak finding (for BLP and LFP lags).

Group level seed-based lag results were obtained in each state (wake and N3/SWS) by computing each quantity at the individual subject level (averaging across temporally contiguous epochs) and then averaging over individuals. Network-level lag analyses (as in Main Text Fig. 4A, 5E, and 6C) were computed by averaging voxel/electrode lag values within network (as defined in Fig. S1). In the ECoG analyses, network-level lags were assessed in an individual only if at least 4 electrodes were present within the network. Thus, not every network was measured in every subject (see Supplemental Figs. S3B, S5B). The language and ventral attention networks were not assessed in the ECoG data due to insufficient coverage.

Participant	Sex	Age	Total wake data (min)	# of wake epochs	Total SWS data (min)	# of SWS epochs	# of electrodes (used/available)	Seizure focus/pathology	Verbal memory impairment
PT 1	M	56	552	89	135	21	38/84	Left lateral anterior temporal lobe; pathology unknown	1+
PT 2	F	60	190	34	199	29	63/102	Right occipital lobe, meningioma	1+
PT 3	M	30	125	9	54	4	52/90	Left superior temporal gyrus; focal cortical dysplasia	0
PT 4	M	19	182	13	49	5	49/88	Right temporal-parietal junction; ganglioglioma	0
PT 5	F	44	657	62	58	6	38/78	Left lateral anterior temporal lobe; focal cortical dysplasia	1+

Table S1: ECoG patient characteristics and experimental data. Subjects were not given anti-epileptic medications during the recording period with the exception of PT 4. PT 4 received 1000mg levetiracetam (Keppra) 1x/day. Verbal memory impairment code: 0: none. 1+: mild list learning deficit in the setting of long-standing anxiety/depression.

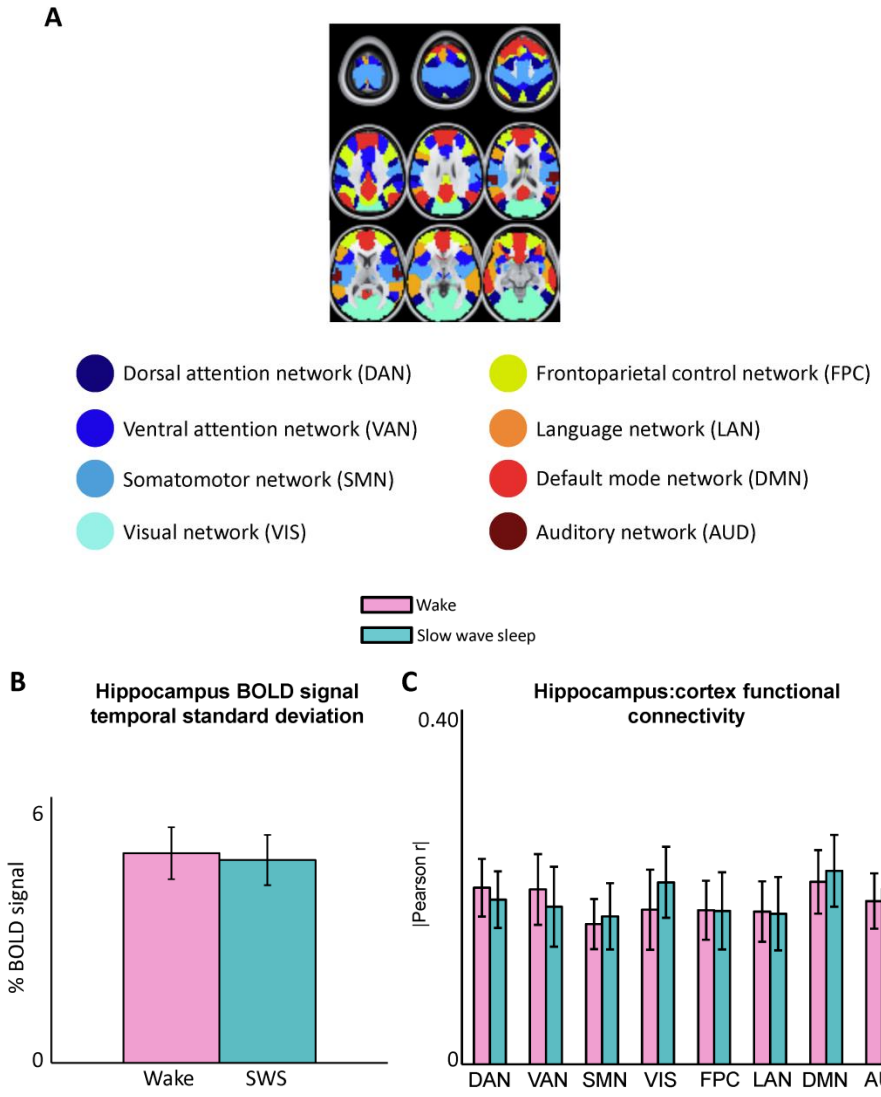

Figure S1: (A): Resting state network (RSN) assignments used in the Main Text. The 8 cortical resting state networks were defined by (Hacker et al., 2013) in a large cohort of awake subjects. As sleep has only minimal effects on correlation structure, we apply the same RSN definitions during both wake and SWS (Mitra et al., 2015b; Picchioni et al., 2013). The color code in this figure is unrelated to latency. (B): BOLD signal amplitude, measured in wake and SWS, in the hippocampus bilateral seed region of interest (shown in Main Text Fig. 2A). Signal amplitude measured by computing temporal standard deviation over time; standard deviation values were averaged over individuals. There is no statistically significant difference in hippocampus BOLD signal amplitude in wake vs. SWS. (C): Zero-lag correlations (functional connectivity), in rs-fMRI, between the hippocampus ROI and each of the cortical networks in (A) in wake and SWS. There is no statistically significant difference in hippocampal functional connectivity in wake vs. SWS.

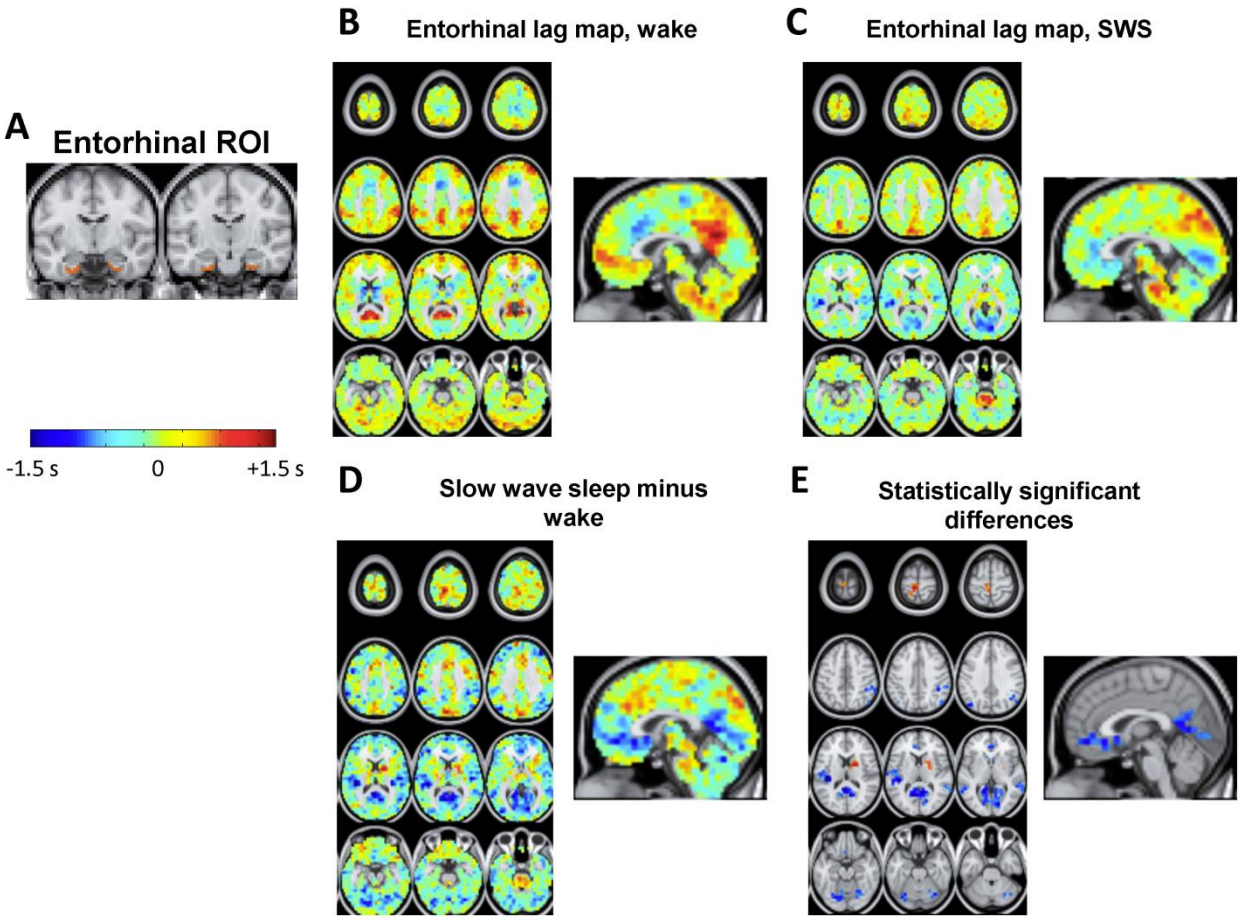

Figure S2: Entorhinal cortex seed-based lag maps in wake and SWS; these analyses mirror the analyses in Main Text Fig. 3, except with respect to an entorhinal rather than hippocampal seed. (A): Bilateral entorhinal seed region. (B)-(C): Entorhinal seed-based lag maps during wake and SWS, respectively. (D) SWS minus wake lag map differences. (E) Difference map in (C) masked for statistical significance at the spatial cluster level ($|Z| > 4.5$, $p < 0.05$ corrected).

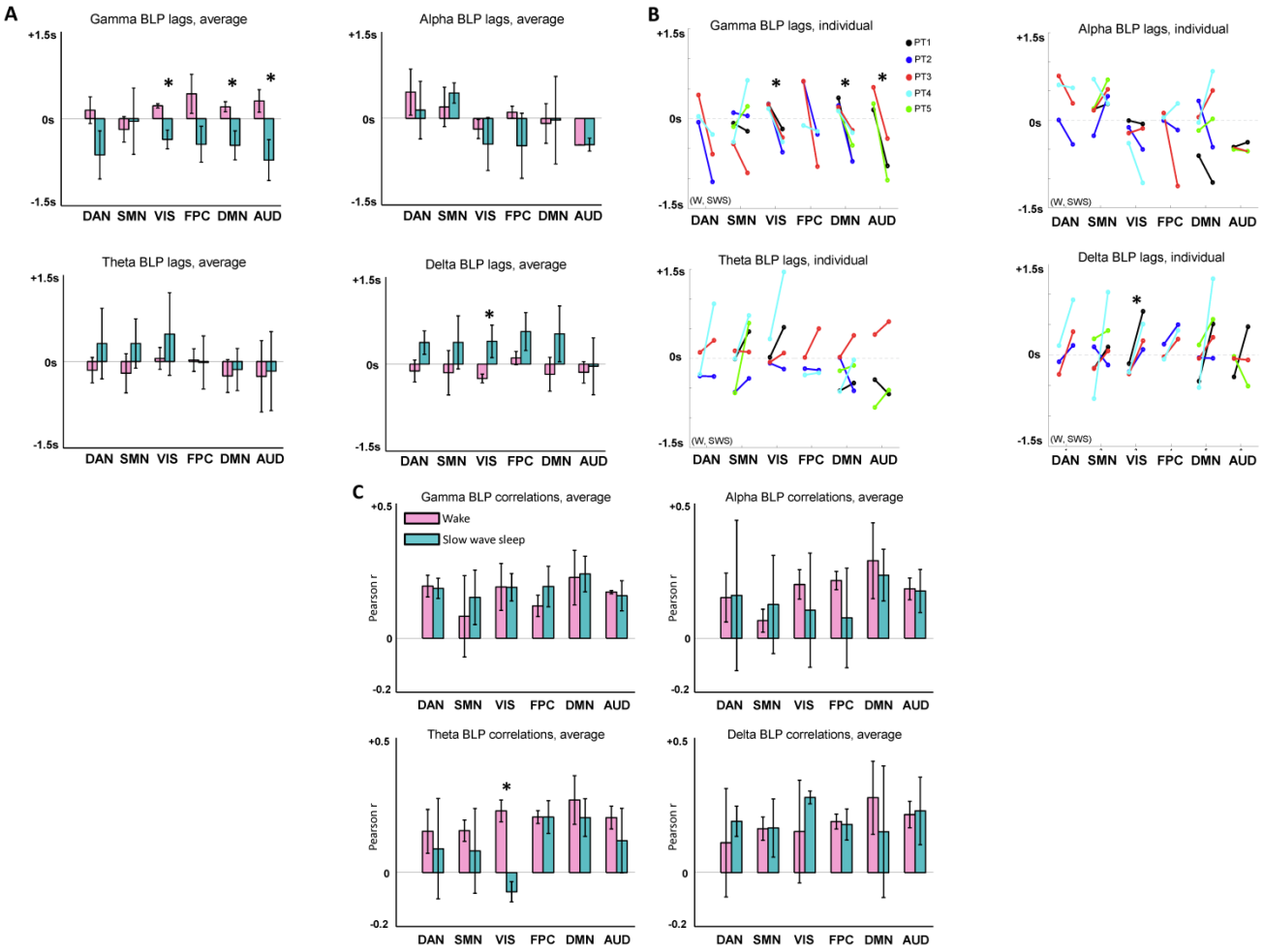

Figure S3: ECoG infra-slow BLP analyses. (A) Mean infra-slow BLP lags between the hippocampus and six cortical networks, parametric in carrier frequency. As shown in Main Text Figure 5, significant lag reversals are present in gamma BLP. No significant reversals were found in alpha or theta BLPs. Interestingly, a trend from "early" to "late", across wake and SWS, is found in delta BLPs. This effect, which is the opposite of the directionality found in gamma BLPs, is significant in the visual network. We have previously found that the temporal structure of rs-fMRI data is composed of multiple temporal sequences, which we have called "lag threads" (Mitra et al., 2015a). The primary rs-fMRI lag thread during wake propagates from the hippocampal system to cerebral cortex, but a second thread in wake propagates in the reverse direction (Mitra et al., 2015a). Speculatively, this observation raises the possibility that gamma and delta BLP lag patterns are correlates of the first and second rs-fMRI lag threads, respectively (see Fig. 2 in (Mitra et al., 2015a)). More broadly, the high dimensionality of rs-fMRI lag structure may arise from multiple patterns of infra-slow propagation differing in carrier frequency. (B) Individual lag results corresponding to panel (A). (C) Zero-lag correlations (functional connectivity), in infra-slow BLPs, between the hippocampus and each of the cortical networks in wake and SWS. There is no statistically significant difference in hippocampal functional connectivity in wake vs. SWS.

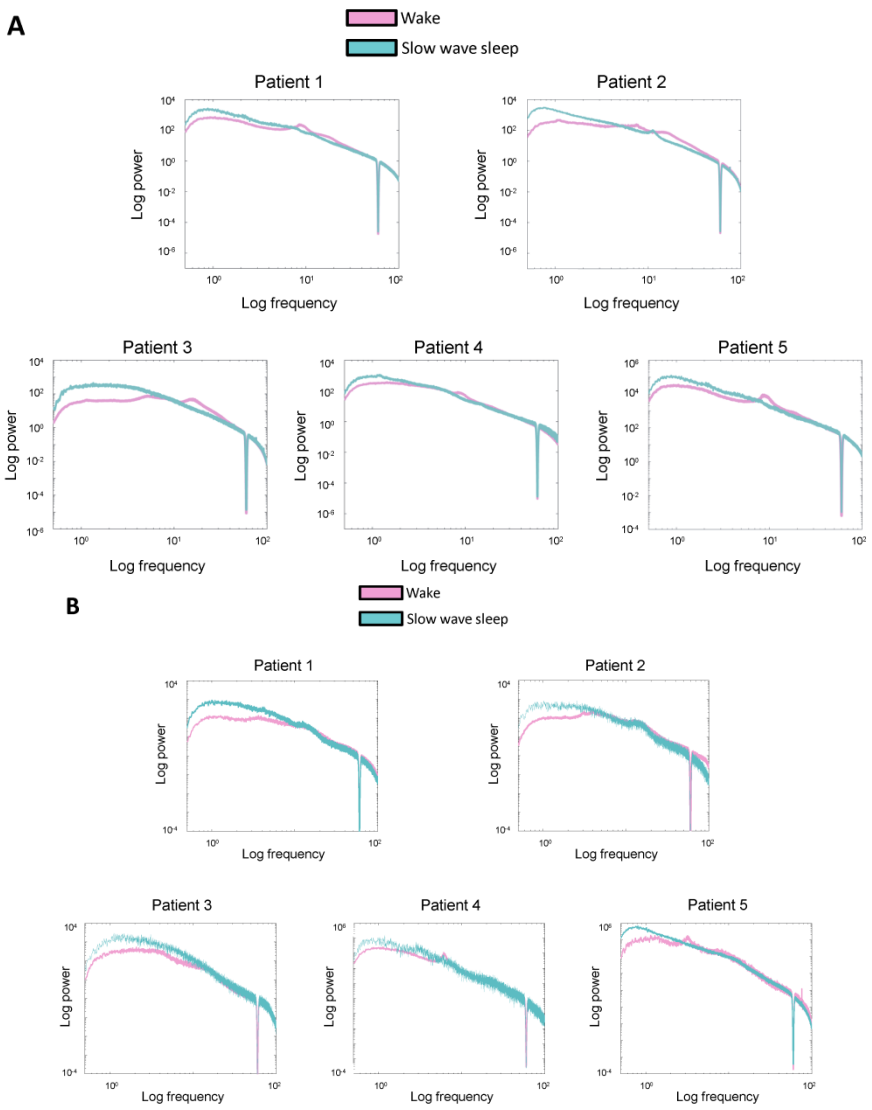

Figure S4: ECoG power spectra in wake and SWS. (A) Power spectrums for analyzed cortical electrodes in each of the 5 subjects included in the analysis. Curves are plotted on a log-log scale, and reflect the average power-spectral density across electrodes and epochs. As expected, low frequency power is substantially higher in temporal epochs classified as SWS as compared to wake. Dip in power at 60 Hz reflects notch-filtering applied to remove 60 Hz noise. (B) Power spectrums for hippocampal electrodes in each of the 5 subjects.

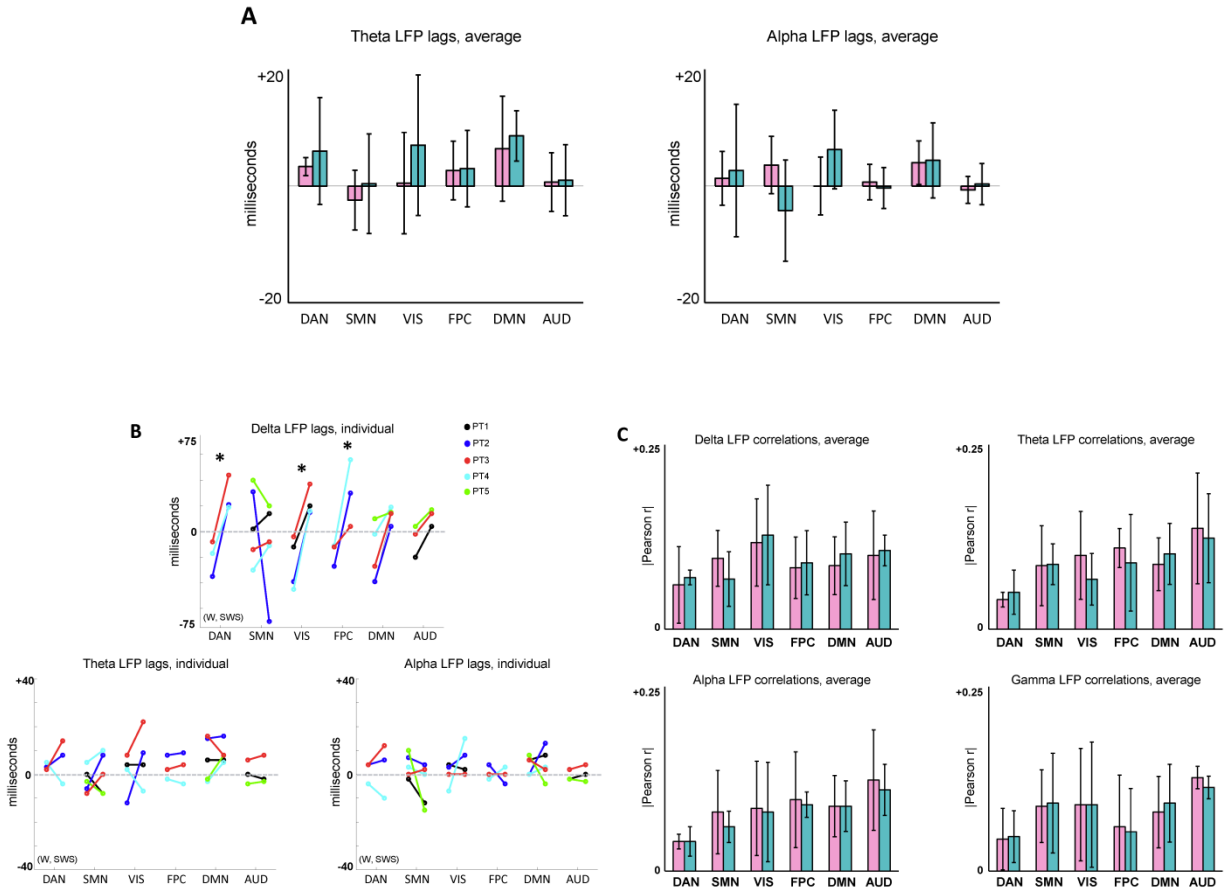

Figure S5: ECoG LFP analyses. (A) Mean LFP lags between the hippocampus and six cortical networks, parametric in carrier frequency. Lags in gamma LFP between the hippocampus and cortex were always zero, and hence not illustrated. No significant reversals were found in alpha or theta LFPs. Delta LFP lags are found in Main Text Figure 6. (B) Individual lag results corresponding to panel (A), including delta LFPs. (C) Zero-lag LFP correlations (functional connectivity) between the hippocampus and each of the cortical networks in wake and SWS. There is no statistically significant difference in hippocampal functional connectivity in wake vs. SWS.

Supplemental References

Foster, B.L., Rangarajan, V., Shirer, W.R., and Parvizi, J. (2015). Intrinsic and task-dependent coupling of neuronal population activity in human parietal cortex. Neuron 86, 578-590.
Fox, M.D., Zhang, D., Snyder, A.Z., and Raichle, M.E. (2009). The global signal and observed anticorrelated resting state brain networks. J Neurophysiol 101, 3270-3283.
Hacker, C.D., Laumann, T.O., Szrama, N.P., Baldassarre, A., Snyder, A.Z., Leuthardt, E.C., and Corbetta, M. (2013). Resting state network estimation in individual subjects. Neuroimage 82C, 616-633.
Hangya, B., Tihanyi, B.T., Entz, L., Fabo, D., Eross, L., Wittner, L., Jakus, R., Varga, V., Freund, T.F., and Ulbert, I. (2011). Complex propagation patterns characterize human cortical activity during slow-wave sleep. J Neurosci 31, 8770-8779.
He, B.J., Snyder, A.Z., Zempel, J.M., Smyth, M.D., and Raichle, M.E. (2008). Electrophysiological correlates of the brain's intrinsic large-scale functional architecture. Proc Natl Acad Sci U S A 105, 16039-16044.
Hermes, D., Miller, K.J., Noordmans, H.J., Vansteensel, M.J., and Ramsey, N.F. (2010). Automated electrocorticographic electrode localization on individually rendered brain surfaces. J Neurosci Methods 185, 293-298.
Iber, C. (2007). The AASM manual for the scoring of sleep and associated events: rules, terminology and technical specifications (American Academy of Sleep Medicine).
Konig, P. (1994). A method for the quantification of synchrony and oscillatory properties of neuronal activity. J Neurosci Methods 54, 31-37.
Mitra, A., Snyder, A.Z., Blazey, T., and Raichle, M.E. (2015a). Lag threads organize the brain's intrinsic activity. Proc Natl Acad Sci U S A 112, E2235-2244.
Mitra, A., Snyder, A.Z., Hacker, C.D., and Raichle, M.E. (2014). Lag structure in resting state fMRI. J Neurophysiol.
Mitra, A., Snyder, A.Z., Tagliazucchi, E., Laufs, H., and Raichle, M.E. (2015b). Propagated infra-slow intrinsic brain activity reorganizes across wake and slow wave sleep. eLife 4.
Picchioni, D., Duyn, J.H., and Horovitz, S.G. (2013). Sleep and the functional connectome. Neuroimage 80, 387-396.
Power, J.D., Barnes, K.A., Snyder, A.Z., Schlaggar, B.L., and Petersen, S.E. (2012). Spurious but systematic correlations in functional connectivity MRI networks arise from subject motion. Neuroimage 59, 2142-2154.

Supplemental Notes Appendix

1. How do the present results relate to previous findings regarding the propagation of delta slow waves (or UP/DOWN states; UDS) during slow wave sleep?

Several previous studies (cited in the main text) have examined propagated activity in the delta range between hippocampus and cortex (Hahn et al., 2012; Isomura et al., 2006; Nir et al., 2011). However, the present analysis technique is quite different from that in previous studies. Previous studies (Hahn et al., 2012; Isomura et al., 2006; Nir et al., 2011) examined cortico-hippocampal relations targeting a specific neural mechanism, the slow oscillation (or Up/Down states) (Steriade et al., 1993). In contrast, the present study does not isolate the slow oscillation, per se. Rather, we analyze propagated LFP activity in a particular spectral band during both wake and SWS. Since much prior work has established that the delta band encompasses multiple neural mechanisms (Amzica and Steriade, 1998), our analysis of whole-band delta activity likely represents a set of processes broader than the slow oscillation. In particular, bursts of delta activity in the hippocampus in waking primates has been associated with functions traditionally assigned to hippocampal theta in rodents (Watrous et al., 2011).

The distinction between delta LFPs, which we investigate, and the slow oscillation is not merely semantic. Although both phenomena have frequency content in the 0.5-4Hz range, one of the characteristic features of Up/Down states (UDS's) is that intra-cellular membrane potentials during UDS oscillations are bi-modal. Indeed, as shown in Figure R1A, intra-cellular Vm histograms measured during the slow oscillation in (Isomura et al., 2006) are bimodal. In contrast, delta LFP activity during slow wave sleep, as measured in the present study, is uni-modal and Gaussian (Fig. R1B). Fig. R1B is derived from SWS, but the results are identical in the wake state.

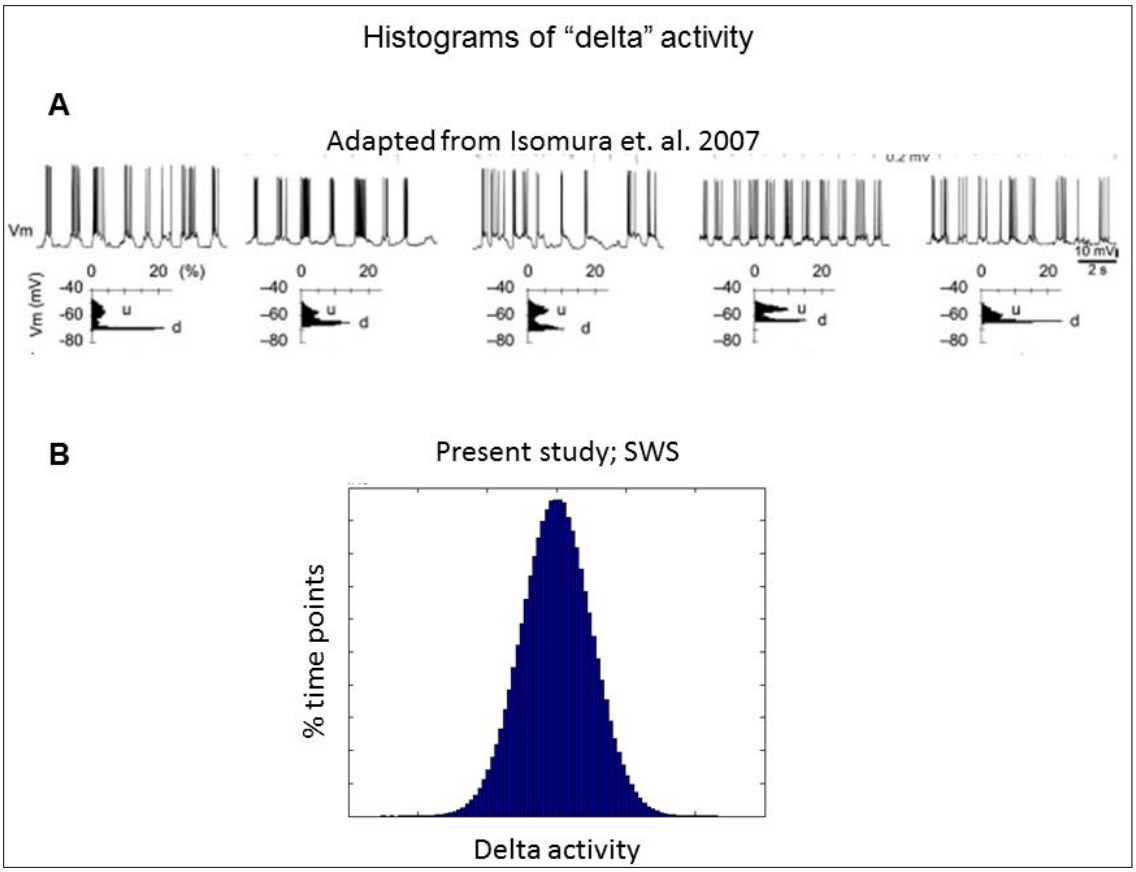

Figure R1

Similar considerations apply when comparing the present results to those reported in Nir 2011. Unlike the present whole-band analysis of delta LFPs, the methodology applied in Nir 2011 identifies specific slow waves for analysis by finding zero-crossings in 0.5-4Hz filtered data of specific temporal lengths (Riedner et al., 2007). The result, as illustrated in Fig. R2, is that only isolated segments of the data are used to compute the direction of propagation between nodes. Moreover, contrasting panels R2A and R2B, the percentage of analyzed data is variable. Fig. R2 is adapted from (Riedner et al., 2007) as similar traces were not available for (Nir et al., 2011). The zero-crossing technique allows the study of a particular neural event, in this case, the slow wave, in service of testing a specific, a priori hypothesis. However, this approach is not well matched to the question in the present study, which instead aims to study propagation within particular spectral bands. Moreover, a strategy that specifically isolates slow waves (Riedner et al., 2007) is not appropriate in the present analysis, which contrasts wake vs. SWS, because slow waves are infrequent during wake.

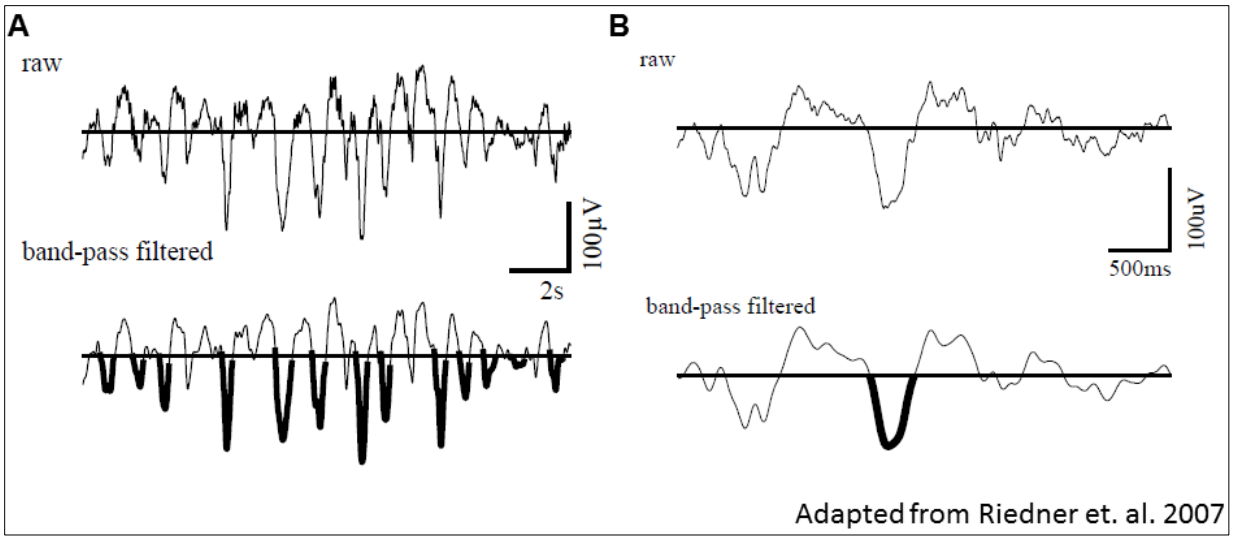

Figure R2

Nevertheless, methodological differences aside, the present results actually agree rather closely with prior work, most of which uses motor areas as a surrogate for cortex in the cortico-hippocampal relationship (Hahn et al., 2006; Isomura et al., 2006; Nir et al., 2011). Indeed, the clearest example of cortex → hippocampus propagation of human slow waves, in Fig. 7A of (Nir et al., 2011), is shown in supplementary motor cortex. Our results agree with this observation; indeed, our main text Figure 7 emphasizes that delta LFPs propagate from the motor system to the hippocampus during SWS.

The question of discrepant observations across studies is complicated by the markedly spatially disjoint electrode coverage between the present study vs. Nir 2011, as illustrated in Fig. R3. Whereas the present ECoG has largely lateral surface coverage (Fig. R3A), Nir 2011 has exclusively medial coverage, including many electrodes in medial motor areas.

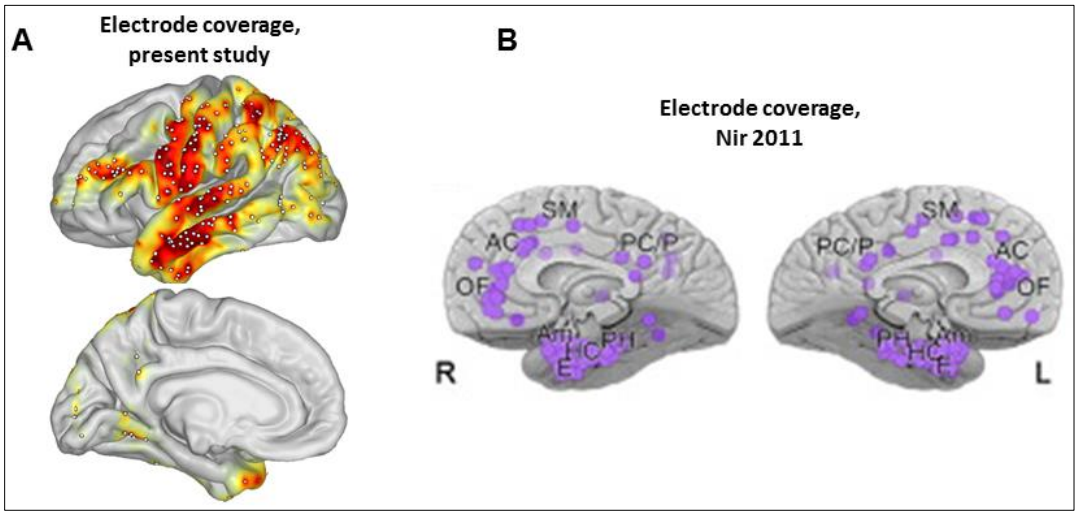

Figure R3

The difference in electrode coverage makes comparing results across the two papers, beyond the motor system, rather difficult. There does seem to be some overlapping coverage across the studies in the posterior cingulate cortex (PCC). Here, there may exist a true discrepancy: we found propagation from hippocampus → PCC in SWS with a 30 msec delay, in contrast to Nir 2011. This difference may be attributable to the analysis of delta LFPs (present study) vs. slow waves (Nir et al., 2011), or simply physiological variability in human epilepsy patients.

2. In Figure 3, an average lag is shown for each and every voxel, but presumably for some voxels there may not be a statistically significant lag (whether positive or negative). What are the statistically significant lags between the hippocampus and the rest of the brain?

It is indeed the case that the full hippocampal lag maps show in main text Figure 3 are not thresholded on the basis of statistical significance. The only clear methodology for accomplishing such a display would rely on parametric cluster-wise statistics. There are a few difficulties with such an approach. First, although we can empirically demonstrate that the distribution of lag values is roughly Gaussian, it is much more difficult to determine whether the distribution of lag cluster sizes is Gaussian. In fact, examining the spatial features in Fig. 3, this is unlikely to be the case. Second, parametric statistics for cluster detection determine whether values are distinguishable from zero; this approach does not distinguish between true zero-lag vs. noisy lags. Third, the analysis of interest in the present paper is the difference between wake and sleep, for which we illustrate a statistically thresholded map in Fig. 4C. In many cases, a statistical difference may appear in regions where no significant lag is detected within state. Such situations make it very difficult to understand the nature of the lag change in a particular location. For these reasons, we have opted to present raw lag maps in main test Fig. 3 absent claims of statistical significance. However, for readers who may be interested, Fig. R4 displays the lag maps in main text Fig. 3 with thresholding for statistical significance ($|Z| > 2.5$, $p < 0.05$ corrected) on the basis of parametric cluster-wise statistics.

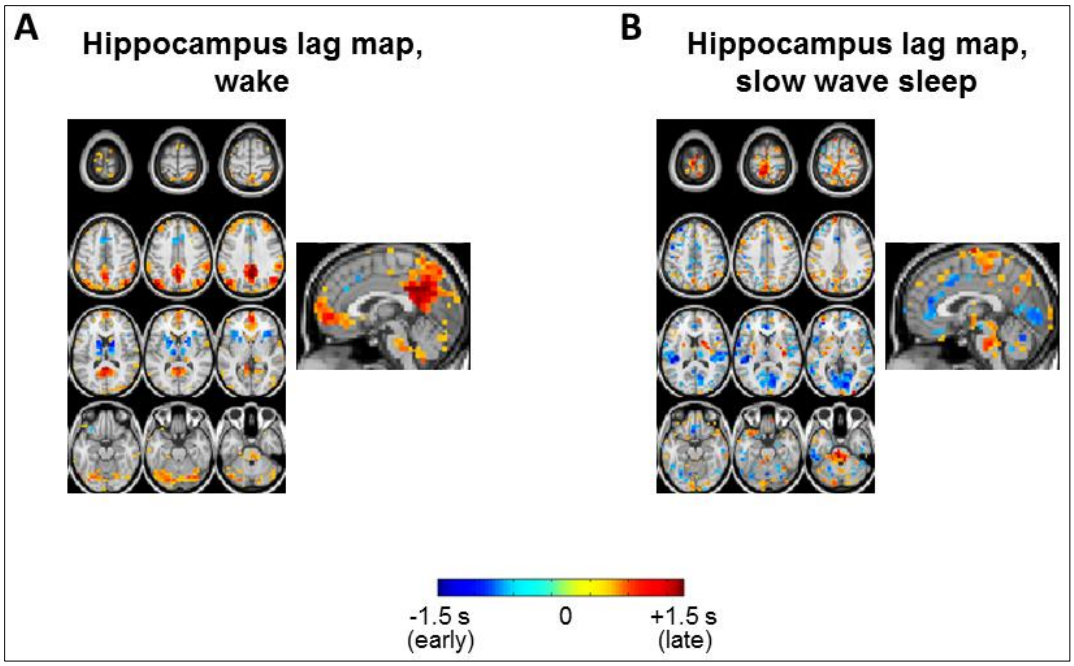

Figure R4

3. How does global signal regression affect analysis of temporal lags?

Although global signal regression (GSR) continues to be a controversial processing step in the analysis of rs-fMRI data, there is increasing agreement that there is significant, widely-distributed artifact in most fMRI recordings, and that GSR is one of the only effective strategies for removing the influence of artifactual signals of non-interest (Power et al., 2013). Thus, if one starts from the premise that the global signal in fMRI is dominated by artifact, all analyses of interest, including temporal lags, should be computed post-GSR.

However, let's examine the worst case scenario: all lags of neural interest are present in the original, pre-GSR data. Fig. R5A illustrates a simple 6-node system in which activity propagates from the first node (blue) to the last (yellow), with a one-unit temporal delay between each node (the specific temporal units are not important; we have simulated aperiodic time series in concordance with BOLD signal spectral content (He et al., 2010)). The global signal for this 6-node system is shown in black at the bottom of Fig. R5A. Now, we regress this global signal from the data to arrive at Fig. R5B. We can verify that the global signal has been removed, as the global signal for the time series depicted in Fig. R5B is identically zero (shown in black). Comparing Fig. R5A vs. R5B, it is clear that the temporal lags structure of the data has been preserved even after GSR. Thus, even in a relatively low-dimensional system, GSR does not materially alter lag structure. Further quantitative confirmation of this impression is shown in Fig. R5C; this panel depicts the lagged correlation function, before and after GSR, between the first and second time series (in blue and green, respectively, in panels A and B). As expected, the magnitude of the correlation between the signals is reduced post GSR.

However, the peak of the lagged correlation function, highlighted by the dashed blue line, remains 1 temporal unit.

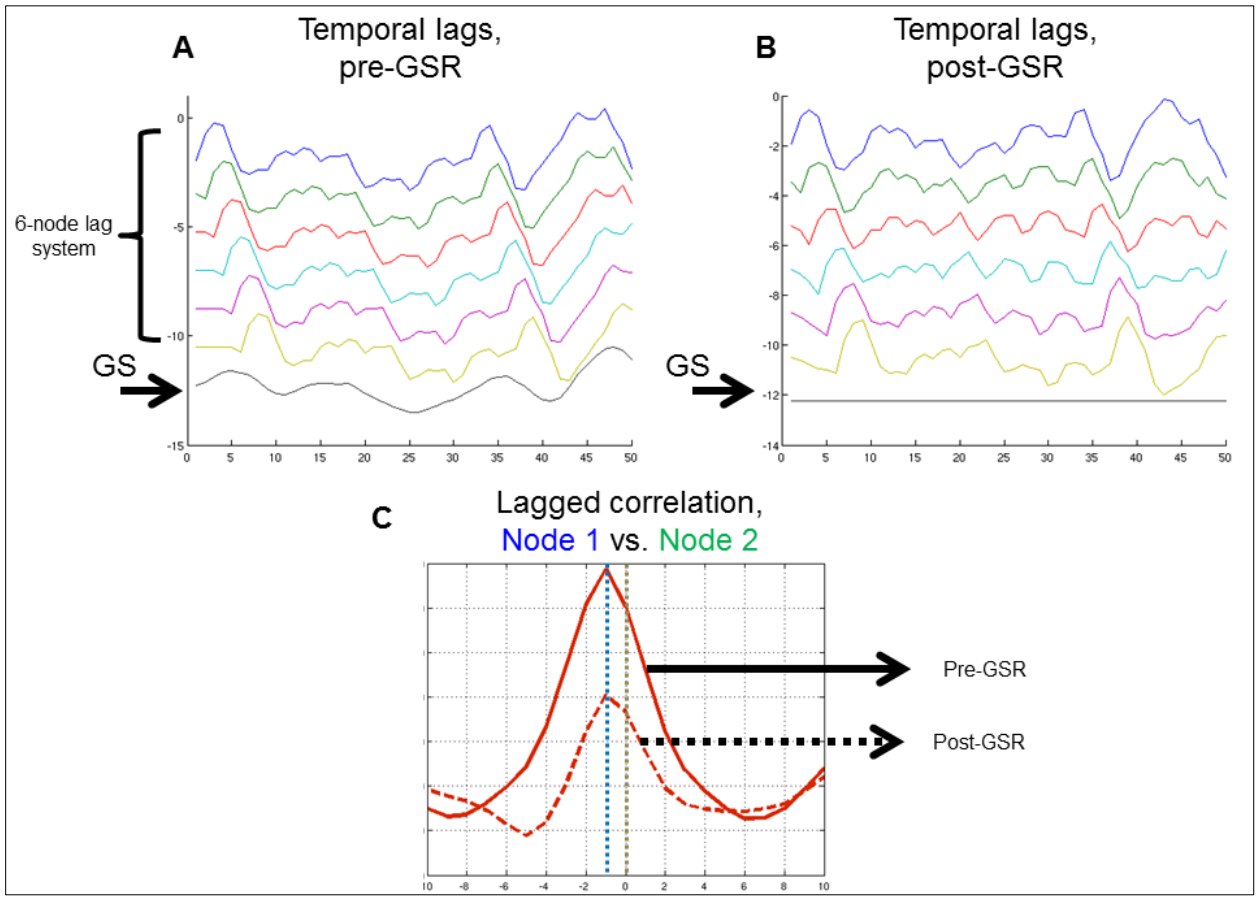

Figure R5

The simulation also answers several other questions. First, this simulation demonstrates global signal regression does not affect a hippocampal seed-based analysis. The full preservation of lag structure means that, for example, all lags with respect to the first (blue) time series are also preserved, even though the first node contributes far less to the global signal than do nodes 2-6 (by definition). Similarly, the fact that the global signal is more reflective of cortex than hippocampus has no bearing on the present analysis. Second, the simulation addresses the appropriateness of computing lags after referencing ECoG data to a common mean. Fig. R5B can be considered ECoG after average referencing, indicating that average referencing need not distort temporal lags.

We emphasize that the simulation presented here does not imply that GSR is unnecessary. Suppose that there were a very high amplitude artifactual spike, lasting several seconds, in the middle of all of the time series in Fig. R5A (e.g., the pre-GSR time series are no longer considered ground truth). Then this massive shared variance would drive the temporal lags toward zero—removing this spike through GSR would

help “uncover” the underlying lag structure. There is good reason to believe this scenario manifests in the rs-fMRI global signal (Power et al., 2013), and the presence of widely shared noise also forms the basis of average-referencing in ECoG (Foster et al., 2015; He et al., 2008).

4. Regarding the estimation of time delays from fMRI BOLD signals, is parabolic interpolation the proper approach for a signal that is shaped more like a gamma function? Does the interpolation rely on only three time points as shown in Figure 2C?

Gamma functions are often used to map between electrophysiogical signals or events and BOLD signals. However, we are not applying parabolic interpolation to the BOLD signal itself; instead, the interpolation is applied to cross-correlation functions computed between pairs of BOLD signals (e.g., main text Fig. 2).

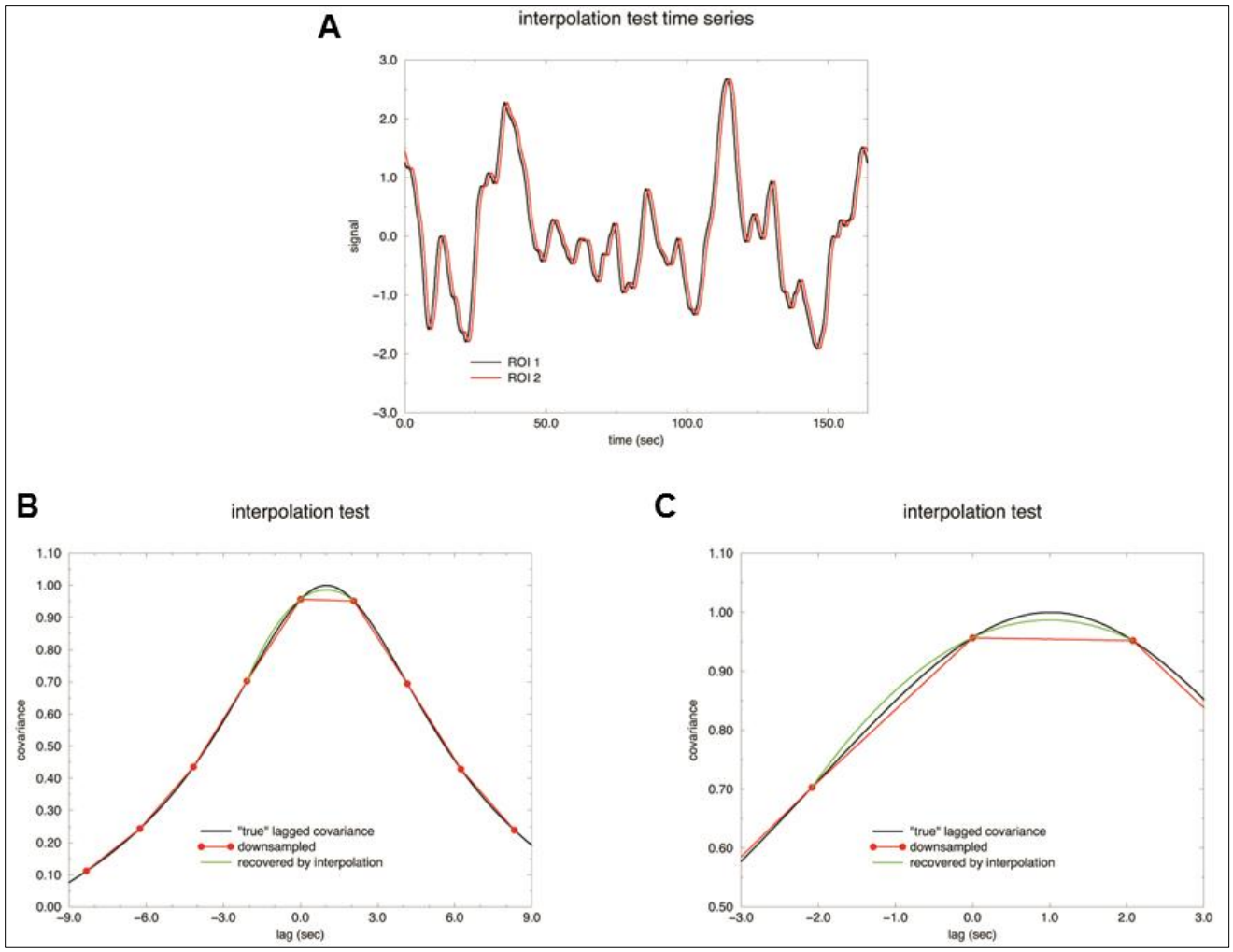

Figure R6

Fig. R6 demonstrates the efficacy of parabolic interpolation directly by simulating BOLD fMRI data at a sampling density of 100 Hz and computing averaged lagged correlation

data at this very high resolution. A lag value of 1.000 sec was simulated. These results then were down sampled to one frame per 2.08 sec, as in the presently analyzed rs-fMRI data. Parabolic interpolation then was applied to the correlation function observed at the fMRI frame rate. Fig. R6A shows the time series simulated over one "run" of 163.84 sec, and Figs. R6A-B illustrate two views of the averaged lagged cross-covariance function (10 "runs" = 27 min of data). The “true” high temporal resolution cross-correlation function is shown in black in Figs. R6A-B; the down-sampled cross-correlation results are in red. The analytic expansion of the parabolic model, derived from the down-sampled data in red, is depicted in green. Over 20 simulated datasets, the mean error in observed peak times (time of green peak vs. black peak) was -0.0074 +/- 0.0055 sec. Although this demonstration omits additive noise, it establishes that parabolic interpolation is an adequate approach for estimating lags in fMRI data.

Finally, we do in fact use three points to fit the parabolic peak of the cross-correlation function. The reason for this choice is apparent from visually inspecting the lagged correlation function shown in Fig. R6B (as well as main text Figs. 2C, 4D-E, and 5D). Note that the lagged correlation functions are quite parabolic near the peak, but that the shapes becomes less parabolic at longer lags (e.g., the flaring of the curve in Fig. R6B). Thus, the peak of the cross-correlation is actually better estimated by only fitting 3 points, as opposed to the entire lagged correlation function. To explore this point quantitatively, we examined the real ECoG data acquired which was acquired at a high sampling rate (infra-slow gamma BLP lagged covariances). In these curves, we empirically know the “real peak”. We then re-sampled the empirical lagged correlation functions to 2.08 secs, as in the simulation in Fig. R6, and applied parabolic interpolation on 3, 5, 7, and 9 points. The mean error in the interpolated peak times were -0.0068 +/- 0.0070 sec, -0.0071 +/- 0.0062 sec, -0.0104 +/- 0.0091 sec, and +0.0500 +/- 0.0120 sec, respectively. Thus, the 3-point interpolation performs best in real data.

6. How stable are haemodynamic response functions across regions in relation to brain state (wake/sleep)? Can neuromodularity systems modify the local BOLD response profile?

Studies of anesthesia in animals suggest that the coupling between electrical activity and the BOLD signal is stable over a wide range of states, ranging from wakefulness to burst suppression (Liu et al., 2011, 2013). However, these studies do not rule out the possibility that there may be local changes in vascular temporal lags. For this reason, we examined the correspondence between temporal lags in BOLD and infra-slow electrophysiology. The general agreement between main text Fig. 4A and 4E suggests that vascular effects are not responsible for the present effects. However, future studies investigating concurrent BOLD and electrophysiology are necessary to understand how the relationship between hemodynamic and electrophysiological signals may be altered under various states.

References for Supplemental Notes

Amzica F, and Steriade M. Electrophysiological correlates of sleep delta waves. *Electroencephalogr Clin Neurophysiol* 107: 69-83, 1998.
Brown RM, and Robertson EM. Off-line processing: reciprocal interactions between declarative and procedural memories. *J Neurosci* 27: 10468-10475, 2007.
Buzsaki G, Kaila K, and Raichle M. Inhibition and brain work. *Neuron* 56: 771-783, 2007.
Buzsaki G, Logothetis N, and Singer W. Scaling brain size, keeping timing: evolutionary preservation of brain rhythms. *Neuron* 80: 751-764, 2013.
Conner CR, Ellmore TM, Pieters TA, DiSano MA, and Tandon N. Variability of the relationship between electrophysiology and BOLD-fMRI across cortical regions in humans. *The Journal of neuroscience : the official journal of the Society for Neuroscience* 31: 12855-12865, 2011.
DeCoteau WE, Thorn C, Gibson DJ, Courtemanche R, Mitra P, Kubota Y, and Graybiel AM. Learning-related coordination of striatal and hippocampal theta rhythms during acquisition of a procedural maze task. *Proc Natl Acad Sci U S A* 104: 5644-5649, 2007.
Eichenbaum H, Otto T, and Cohen NJ. The hippocampus--what does it do? *Behavioral and neural biology* 57: 2-36, 1992.
Foster BL, Rangarajan V, Shirer WR, and Parvizi J. Intrinsic and task-dependent coupling of neuronal population activity in human parietal cortex. *Neuron* 86: 578-590, 2015.
Friston KJ, and Dolan RJ. Computational and dynamic models in neuroimaging. *Neuroimage* 52: 752-765, 2010.
Hacker CD, Perlmutter JS, Criswell SR, Ances BM, and Snyder AZ. Resting state functional connectivity of the striatum in Parkinson's disease. *Brain : a journal of neurology* 135: 3699-3711, 2012.
Hahn TT, McFarland JM, Berberich S, Sakmann B, and Mehta MR. Spontaneous persistent activity in entorhinal cortex modulates cortico-hippocampal interaction in vivo. *Nat Neurosci* 15: 1531-1538, 2012.
Hahn TT, Sakmann B, and Mehta MR. Phase-locking of hippocampal interneurons' membrane potential to neocortical up-down states. *Nat Neurosci* 9: 1359-1361, 2006.
Handwerker DA, Ollinger JM, and D'Esposito M. Variation of BOLD hemodynamic responses across subjects and brain regions and their effects on statistical analyses. *Neuroimage* 21: 1639-1651, 2004.
Hangya B, Tihanyi BT, Entz L, Fabo D, Eross L, Wittner L, Jakus R, Varga V, Freund TF, and Ulbert I. Complex propagation patterns characterize human cortical activity during slow-wave sleep. *J Neurosci* 31: 8770-8779, 2011.
Hasselmo ME. Neuromodulation: acetylcholine and memory consolidation. *Trends Cogn Sci* 3: 351-359, 1999.
Hayasaka S, and Nichols TE. Validating cluster size inference: random field and permutation methods. *Neuroimage* 20: 2343-2356, 2003.
He BJ, Snyder AZ, Zempel JM, Smyth MD, and Raichle ME. Electrophysiological correlates of the brain's intrinsic large-scale functional architecture. *Proc Natl Acad Sci U S A* 105: 16039-16044, 2008.
He BJ, Zempel JM, Snyder AZ, and Raichle ME. The temporal structures and functional significance of scale-free brain activity. *Neuron* 66: 353-369, 2010.
Iber C. *The AASM manual for the scoring of sleep and associated events: rules, terminology and technical specifications*. American Academy of Sleep Medicine, 2007.
Isomura Y, Sirota A, Ozen S, Montgomery S, Mizuseki K, Henze DA, and Buzsaki G. Integration and segregation of activity in entorhinal-hippocampal subregions by neocortical slow oscillations. *Neuron* 52: 871-882, 2006.
Ji D, and Wilson MA. Coordinated memory replay in the visual cortex and hippocampus during sleep. *Nat Neurosci* 10: 100-107, 2007.
Kayser C, Kim M, Ugurbil K, Kim DS, and Konig P. A comparison of hemodynamic and neural responses in cat visual cortex using complex stimuli. *Cereb Cortex* 14: 881-891, 2004.

Liu X, Yanagawa T, Leopold DA, Fujii N, and Duyn JH. Robust Long-Range Coordination of Spontaneous Neural Activity in Waking, Sleep and Anesthesia. *Cereb Cortex* 2014.
Liu X, Zhu XH, Zhang Y, and Chen W. The change of functional connectivity specificity in rats under various anesthesia levels and its neural origin. *Brain topography* 26: 363-377, 2013.
Liu X, Zhu XH, Zhang Y, and Chen W. Neural origin of spontaneous hemodynamic fluctuations in rats under burst-suppression anesthesia condition. *Cereb Cortex* 21: 374-384, 2011.
Logothetis NK, Eschenko O, Murayama Y, Augath M, Steudel T, Evrard HC, Besserve M, and Oeltermann A. Hippocampal-cortical interaction during periods of subcortical silence. *Nature* 491: 547-553, 2012.
Magri C, Schridde U, Murayama Y, Panzeri S, and Logothetis NK. The amplitude and timing of the BOLD signal reflects the relationship between local field potential power at different frequencies. *The Journal of neuroscience : the official journal of the Society for Neuroscience* 32: 1395-1407, 2012.
McNaughton BL, Barnes CA, Battaglia FP, Bower MR, Cowen SL, Ekstrom AD, Gerrard JL, Hoffman KL, Houston FP, Karten Y, Lipa P, Pennartz CMA, and Sutherland GR. Off-Line Reprocessing of Recent Memory and its Role in Memory Consolidation: A Progress Report. In: *Sleep and Brain Plasticity*, edited by Maquet P, Smith C, and Stickgold RUniversity Press Scholarship Online, 2003.
Mitra A, Snyder AZ, Blazey T, and Raichle ME. Lag threads organize the brain's intrinsic activity. *Proc Natl Acad Sci U S A* 112: E2235-2244, 2015a.
Mitra A, Snyder AZ, Hacker CD, and Raichle ME. Lag structure in resting-state fMRI. *J Neurophysiol* 111: 2374-2391, 2014.
Mitra A, Snyder AZ, Tagliazucchi E, Laufs H, and Raichle ME. Propagated infra-slow intrinsic brain activity reorganizes across wake and slow wave sleep. *eLife* 4: 2015b.
Nir Y, Mukamel R, Dinstein I, Privman E, Harel M, Fisch L, Gelbard-Sagiv H, Kipervasser S, Andelman F, Neufeld MY, Kramer U, Arieli A, Fried I, and Malach R. Interhemispheric correlations of slow spontaneous neuronal fluctuations revealed in human sensory cortex. *Nat Neurosci* 11: 1100-1108, 2008.
Nir Y, Staba RJ, Andrillon T, Vyazovskiy VV, Cirelli C, Fried I, and Tononi G. Regional slow waves and spindles in human sleep. *Neuron* 70: 153-169, 2011.
Ojemann GA, Ojemann J, and Ramsey NF. Relation between functional magnetic resonance imaging (fMRI) and single neuron, local field potential (LFP) and electrocorticography (ECoG) activity in human cortex. *Front Hum Neurosci* 7: 34, 2013.
Picchioni D, Duyn JH, and Horovitz SG. Sleep and the functional connectome. *Neuroimage* 80: 387-396, 2013.
Power JD, Mitra A, Laumann TO, Snyder AZ, Schlaggar BL, and Petersen SE. Methods to detect, characterize, and remove motion artifact in resting state fMRI. *Neuroimage* 84C: 320-341, 2013.
Riedner BA, Vyazovskiy VV, Huber R, Massimini M, Esser S, Murphy M, and Tononi G. Sleep homeostasis and cortical synchronization: III. A high-density EEG study of sleep slow waves in humans. *Sleep* 30: 1643-1657, 2007.
Seger CA, and Cincotta CM. Dynamics of frontal, striatal, and hippocampal systems during rule learning. *Cereb Cortex* 16: 1546-1555, 2006.
Sirota A, Csicsvari J, Buhl D, and Buzsaki G. Communication between neocortex and hippocampus during sleep in rodents. *Proc Natl Acad Sci U S A* 100: 2065-2069, 2003.
Sirota A, Montgomery S, Fujisawa S, Isomura Y, Zugaro M, and Buzsaki G. Entrainment of neocortical neurons and gamma oscillations by the hippocampal theta rhythm. *Neuron* 60: 683-697, 2008.
Steriade M, Nunez A, and Amzica F. A novel slow (< 1 Hz) oscillation of neocortical neurons in vivo: depolarizing and hyperpolarizing components. *J Neurosci* 13: 3252-3265, 1993.
Stickgold R. Sleep-dependent memory consolidation. *Nature* 437: 1272-1278, 2005.

Tagliazucchi E, von Wegner F, Morzelewski A, Brodbeck V, Jahnke K, and Laufs H. Breakdown of long-range temporal dependence in default mode and attention networks during deep sleep. *Proc Natl Acad Sci U S A* 110: 15419-15424, 2013.
Watrous AJ, Fried I, and Ekstrom AD. Behavioral correlates of human hippocampal delta and theta oscillations during navigation. *J Neurophysiol* 105: 1747-1755, 2011.